Research Square

Preprints are preliminary reports that have not undergone peer review.
They should not be considered conclusive, used to inform clinical practice,
or referenced by the media as validated information.

Comparative analysis of Different Closed-loop Borehole Heat Exchanger Thermal Performance in shallow High-Temperature Environment

DAN AZIMI MOHAMAN

mohaman.danazimi@studenti.unipd.it

University of Padua

Monia Procesi

National Institute of Geophysics and Volcanology

Eloisa Di Sipio

University of Padua

Giorgia Dalla Santa

University of Padua

Paolo Scotton

University of Padua

Antonio Galgaro

University of Padua

Research Article

Keywords: Closed-loop geothermal system, Coaxial borehole heat exchanger, Horizontal well, multilateral well, Heat transfer numerical modelling, Renewable energy, Island decarbonization

Posted Date: February 26th, 2026

DOI: https://doi.org/10.21203/rs.3.rs-8927294/v1

License: This work is licensed under a Creative Commons Attribution 4.0 International License.
Read Full License

Additional Declarations: No competing interests reported.

Comparative analysis of Different Closed-loop Borehole Heat Exchanger Thermal Performance in shallow High-Temperature Environment

Abstract

Closed-loop geothermal systems offer a promising pathway for exploiting high geothermal gradients in volcanic environments while avoiding the operational and environmental risks associated with open-loop circulation. However, the influence of borehole trajectory and geometric configuration on the long-term thermal performance of such systems remains insufficiently constrained, particularly under shallow, high-temperature volcanic conditions. This study presents a systematic numerical comparison of five closed-loop borehole heat exchanger (CBHE) configurations: i) vertical coaxial (V-CBHE), ii) deviated coaxial (D-CBHE), iii) horizontal coaxial (H-CBHE), iv) U-loop (U-CBHE), and v) single-lateral (SL-CBHE), using geological and thermal conditions representative of Vulcano Island (Italy). A fully coupled 1D wellbore–3D formation thermo-hydraulic model was developed in a FEM commercial software to simulate conductive heat transfer and fluid circulation over a 25-year operational period. Sensitivity analyses were conducted to evaluate the effects of borehole geometry, inclination depth and angle, horizontal extension length, injection temperature, flow rate, and insulation strategies. Results demonstrate that borehole geometry exerts a dominant control on long-term performance, surpassing the influence of operational parameters. Lateral configurations significantly outperform vertical and deviated systems by extending heat-exchange length within high-temperature formations, increasing fluid residence time, and distributing thermal drawdown over a larger rock volume. After 25 years of continuous operation, horizontal, U-loop, and single-lateral systems stabilise at production temperatures of approximately 147–165 °C, compared to 96–101 °C for vertical and deviated configurations. Inner-pipe insulation effectively mitigates internal thermal short-circuiting, particularly during early operation. Although electrical power estimates represent idealised upper bounds, the relative performance ranking among configurations remains robust. These findings highlight

trajectory design as a critical lever for optimising closed-loop geothermal systems in shallow, high-enthalpy volcanic environments.

Keywords: Closed-loop geothermal system; Coaxial borehole heat exchanger; Horizontal well; multilateral well; Heat transfer numerical modelling, Renewable energy, Island decarbonization.

1. Introduction

The growing energy demand in isolated island regions, coupled with their heavy reliance on fossil fuels, has intensified the search for low-carbon and locally available energy solutions. In particular, on volcanic islands, the elevated geothermal gradients commonly present at shallow depths make geothermal energy a particularly promising alternative energy source (Durga et al., 2021; Gluyas et al., 2018) [1,2]. Although policy support and technological innovation have enhanced renewable energy integration (GENI. (2008); Kuang et al., 2016) [3,4], space constraints often limit the large-scale deployment of solar and wind infrastructure. For volcanic islands, geothermal energy emerges as an alternative baseload, clean and weather-independent renewable energy source (Nakomcic-Smaragdakis et al., 2016) [5]. Geothermal exploitation can broadly be classified into shallow, near-surface systems and deep systems accessed through deep drilling (Soltani et al., 2019) [6]. Development approaches are further divided into open-loop and closed-loop geothermal systems. Open-loop systems comprising single-well open-loop and enhanced geothermal systems (EGS) extract subsurface fluids to generate electricity and subsequently reinject or dispose of these fluids at surface (Wang et al., 2020) [7]. Though these systems face challenges such as reservoir depletion, high water consumption, and environmental impacts (Glassley et al., 2014) [8]. In addition, EGS technologies present challenges like induced seismicity, fluid loss, and technical complexity (Shi et al., 2019; Pruess, 2006; Chenet al., 2019; Giardini, 2009; Anderson at al., 2019) [9-13]. Closed-loop geothermal systems, which circulate a working fluid through sealed piping without contact with the subsurface environment, offer a low-risk alternative that avoids hydraulic fracturing (Wanget al., 2021; Holmberg et al., 2016) [14;15]. Numerous studies have examined their heat-extraction behaviour: Dai et al. (2019) [16] conducted field tests on a deep coaxial open-loop system, while Wang et al. (2019) [17] developed a three-dimensional numerical model analysing the influence of fluid flow rate and injection–production intervals on system

performance. Building on this, innovative well architectures such as horizontal wells (Wang et al., 2020) [18] and multi-well systems (Wang et al., 2022) [19] have been proposed to enhance productivity. Within EGS applications, stimulation of hot dry rock reservoirs has received significant attention. Novel well designs including horizontal wells (Yu et al., 2021) [20] and pinnate horizontal wells (Xie et al., 2022) [21] demonstrate enhanced thermal performance. Nonetheless, EGS deployment remains constrained by issues such as induced seismicity (Pasqualetti, 1980; Bayer et al., 2013) [22,23], high geological uncertainty, substantial upfront drilling costs (Soltani et al., 2021) [24] and application limitation in some countries, such as Italy.

Closed-loop geothermal systems offer an alternative in which working fluids circulate within sealed wellbore heat exchangers without direct interaction with reservoir fluids. Heat is transferred conductively through the wellbore wall from the surrounding formation. Prior studies have explored various aspects of closed-loop performance, including field- and simulation-based investigations of deep ground-source heat pump systems (Wang et al., 2017) [25], evaluations of single-well performance in volcanic settings (Renaud et al., 2019) [26], and transient three-dimensional modelling of coaxial heat exchangers (Zhang et al., 2019) [27]. Recent advancements include segmented material designs tailored to geothermal gradient variations (Luo et al., 2024) [28], thermal-resistance-based performance assessments (Guo et al., 2024) [29], and comparisons of CO_2 and water as working fluids (Bai et al., 2022) [30]. Additional work has considered intermittent operating modes (Deng et al., 2023) [31], the influence of cement thermal conductivity (Song et al., 2018) [32], and the impacts of gravity and viscous friction on system economics (Wang et al., 2020) [18]. Although inherently safer and operationally simpler than open-loop alternatives, closed-loop systems often exhibit comparatively lower extraction rates due to limited thermal contact area and slower rock-to-wellbore heat transfer (Beckers et al., 2022) [33]. To address these limitations, recent

researches have focused on increasing the efficiency of coaxial heat exchangers through geometric or material innovations, such as inner-tube spiral fins (Liu et al., 2023, 2024, 2023) [34–36] and elliptical outer tubes (Rajeh et al., 2023, 2024) [37,38].

Horizontal well technology extensively applied in the oil and gas industry has also attracted growing interest for geothermal applications (Mao et al., 2018) [39]. Novel horizontal coaxial geothermal systems have been proposed and validated via field testing and numerical simulations (Guo et al., 2024; Akram et al., 2024) [29,40]. Wang et al. (2021) [7] demonstrated that a 2000 m horizontal section can increase outlet temperature by roughly 20°C, corresponding to a thermal power gain of approximately 0.96 MW. More detailed studies of horizontal and multi-well coaxial closed-loop geothermal systems (Wang et al., 2021; 2021) [14,41] showed that long horizontal laterals enable more effective utilisation of reservoir heat than purely vertical wells. Additional enhancements include horizontal DBHE configurations (Liu et al., 2023) [42], insulated hydraulic fractures to enlarge heat-exchange area (Liu et al., 2024) [43], and multilateral coaxial systems exhibiting markedly improved heat absorption per unit length (Esmaeilpour et al., 2023) [44]. A key development in this field is the emergence of deep multilateral closed-loop systems, exemplified by the Eavor-Loop concept, which employs branched or folded lateral arrays connected to shared vertical wells and relies on conduction-driven heat uptake enhanced by thermosiphon effects. Numerical modelling of such systems demonstrates that multilateral configurations can increase heat extraction relative to single-well DBHEs, though performance is strongly influenced by rock thermal conductivity, thermal interference among branches, groundwater movement, and achievable production temperatures (Kelly & McDermott, 2022) [45].

The reviewed literature indicates a dominant focus on deep coaxial borehole heat exchangers (DBHEs), typically extending several kilometres. Far fewer studies have examined shallow closed-loop systems in volcanic insular settings, where geometry: vertical, deviated, horizontal,

U-loop and single-lateral becomes critical for maximizing thermal contact within elevated temperature zones. Purely vertical systems rely solely on depth to access elevated undisturbed ground temperatures, whereas deviated, horizontal, U-loop and single-lateral geometries can extend contact length within hotter layers, potentially improving heat extraction by increasing fluid residence time and effective thermal interaction. Deviated, horizontal, U-loop and single-lateral closed-loop borehole heat exchanger thus represent a promising but understudied configuration. Their deployment, however, introduces additional complexities, including drilling challenges, increased riser heat losses, and altered long-term thermal recharge behaviour.

To address these gaps, the present study provides a systematic comparison of the long-term thermal performance of vertical, deviated, horizontal, U-loop and single-lateral closed-loop heat-exchanger configurations under shallow, high-temperature volcanic conditions representative of Mediterranean island settings such as Vulcano, Italy. The objectives of this work are to (i) quantify the long-term thermal performance of different CBHE geometries under identical geological and operational conditions, (ii) evaluate the relative influence of geometric versus operational parameters on production temperature and heat extraction, and (iii) derive geometry-driven design insights relevant to the deployment of closed-loop geothermal systems in shallow, high-enthalpy volcanic environments. While the results are not intended as site-specific production forecasts, they may provide a comparative framework to guide system design and technology selection for volcanic island decarbonisation strategies.

2. Methodology

Vulcano is an active volcanic island in the Aeolian Archipelago (southern Tyrrhenian Sea, Italy), characterized by intense fumarolic activity, shallow hydrothermal circulation, and high heat flux, and is part of one of the most active volcanic systems in the Mediterranean. Past

geothermal exploration was conducted in the 1950s by the drilling of two shallow wells to depths of approximately 200 m, which revealed extremely high temperatures at shallow depth (about 200°C) resulting from the superposition of deep magmatic heat input and shallow hydrothermal circulation (Sommaruga, 1984) [46]. Subsequent exploration was carried out during the 1980s involved deeper wells reaching depths of 1700–2000 m. These wells encountered very high temperatures starting from 600 depth, documenting a vertical decoupling between shallow, permeable hydrothermal circulation and deeper, conduction-dominated thermal regimes. This evidence supports the coexistence of convective heat transfer at shallow levels and predominantly conductive heat transfer at greater depths (Todesco, 1997) [47]. Importantly, available temperature profiles indicate a rapid increase in formation temperature within the upper few hundred metres, although the underlying heat-transfer mechanisms vary spatially and temporally due to fracture-controlled fluid flow, boiling processes, and permeability heterogeneity. Accordingly, this study employs a simplified stratigraphic and thermal framework that captures the elevated shallow temperatures documented by historical drilling, while neglecting fluid flow within the formation. The subsurface is represented by five lithological units corresponding to the dominant volcanic and volcaniclastic formations at shallow depth, with thermophysical properties consistent with hydrothermally altered volcanic rocks reported in the literature (Mohaman et al., 2025) [48]. The primary objective of this study is not to reproduce the natural heat-transfer processes at Vulcano, but to provide a physically realistic boundary condition for evaluating the influence of borehole geometry and trajectory on the long-term thermal performance of closed-loop geothermal systems operating under shallow, high-temperature volcanic conditions.

2.1.Physical model

Coaxial closed-loop geothermal system comprises an inner pipe, an outer pipe, surrounding cement grout and the geothermal reservoir. Two flow paths of the heat carrier fluid can be defined. The fluid can be injected through the annulus section space and flows out from the internal pipe after full heat transfer or vice versa. The structural and operational principles of the four closed-loop geothermal system configurations are illustrated in Figure 1(a-g). The first configuration (Figure 1a) refers to a simple vertical coaxial closed-loop heat exchanger (V-CBHE). In the oil industry, directional drilling refers to the technique of drilling wells that combine vertical sections with smoothly curved sections, typically featuring a constant radius of curvature (Teodoriu & Bello, 2021) [49]. These curved sections exhibit a uniformly changing inclination, typically ranging between 30° and 60°, but can reach up to 90° where necessary (Eren & Suicmez, 2020; Wísniowski et al., 2020) [50,51]. After the curved section, the wellbore often continues in a straight section, maintaining a constant angle. Figure 1b represent a deviated coaxial closed-loop heat exchanger (D-CBHE). In Figures 1c, the vertical and horizontal sections are joined by a deviated section, gradually reaching a maximum angle of 45° before transitioning to a 90° angle within the horizontal segment forming-up a horizontal coaxial borehole heat exchanger (H-CBHE). U-loop closed-loop borehole heat exchanger (U-CBHE) is represented in Figure 1d, it is made of two vertical borehole inlet and outlet connected by a horizontal well forming a closed circuit. Single-lateral closed-loop heat exchanger (SL-CBHE) is made of two parallel lateral wells connected to two vertical borehole inlet and outlet with forming a closed circulation path (Figure 1e). A spacing of 100 m is maintained both between the vertical wells and between the upper and lower lateral wells. These designs form a closed-loop heat exchanger allowing the heat carrier fluid to circulate internally without direct contact with the underground environment. The heat transfer process of the above heat exchanger configuration is mainly divided into heat conduction between reservoir and borehole wall, heat conduction inside pipe wall and grout, convection heat

transfer between circulating fluid and inside and outside pipe surface. Figure 1f and Figure 1g respectively shows the cut plane section of coaxial and the single lateral CBHEs. The modelled borehole depth for all configurations is 400 m. Detailed geometric and material parameters are provided in Tables 1-3.

Table 1. Properties of coaxial borehole heat exchanger.

Parameter	Value
Borehole depth, m	400
Inner pipe outer diameter (D2), mm	120.9
Outer pipe outer diameter (D4), mm	323
Inner pipe thickness (t_i), mm	8.05
Outer pipe thickness (t_o), mm	10.45
Borehole diameter (D6) from 0-50 m depth, mm	473
Borehole diameter (D5) from 50-400 m depth, mm	444
Borehole thickness (t_{b1}) from 0-50 m depth, mm	75
Borehole thickness (t_{b2}) from 50-400 m depth, mm	60.5
Simulation area depth, m	600
Simulation Radius of geometry, m	200

Table 2. Borehole thermal and physical parameters

Lithology area	λ [W/(m·K)]	ρ [kg/m³]	Cp [J/(kg·K)]
Inner pipe	0.18	1190	1470
Outer pipe	15.0	8000	500
Grout	1.50	2300	880

Table 3. Lithological thermal and physical parameters representative of the shallow sequence of Vulcano Island (Mohaman et al. (2025) [48],).

Lithology area	Thickness [m]	λ [W/(m·K)]	ρ [kg/m³]	Cp [J/(kg·K)]
Layer 1	00-150	1.42	2249	200
Layer 2	150-190	1.47	2623	920
Layer 3	190-260	1.05	1170	850
Layer 4	260-350	1.02	1665	850
Layer 5	350-500	2.15	2806	2390

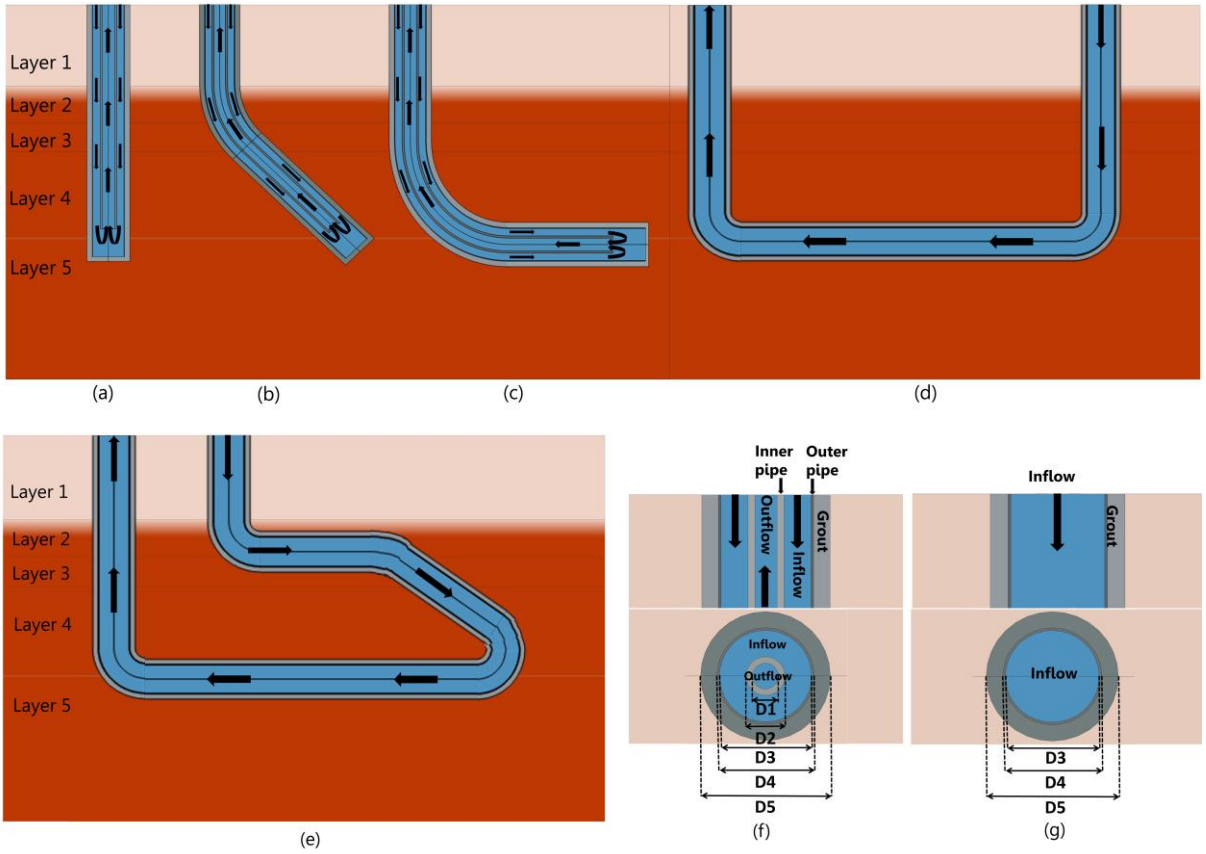


Figure 1. Schematic of the closed-loop borehole heat exchanger systems structure and operating principle: (a) V-CBHE; (b) D-CBHE; (c) H-CBHE; (d) U-CBHE; (e) SL-CBHE; (f) Cut plane section and top view coaxial CBHE; (g) Cut plane section and top view single lateral CBHE.

2.2. Numerical modelling

Numerical simulations were performed using COMSOL Multiphysics (Introduction to COMSOL Multiphysics, 2024) [52], a commercial finite-element software widely used for coupled Multiphysics analyses. COMSOL enables simultaneous simulation of thermal, hydraulic and, where necessary, mechanical processes within a unified modelling environment an essential capability for geothermal system studies, where interactions between fluid flow, heat transfer, and geological media are inherently coupled (Pryor, 2011) [53]. A fully coupled numerical model is developed to simulate fluid circulation and heat transfer within the CBHE and surrounding formation. The modelling framework consists of one-dimensional non-isothermal pipe flow within the closed-loop borehole and three-dimensional conductive heat transfer within the formation (Figure 3.2). Five CBHE configurations vertical, deviated, horizontal, U-Single lateral and Single lateral wells were developed and examined. Figure 3.2 illustrates the numerical modelling flow chart used to build and set up the models.

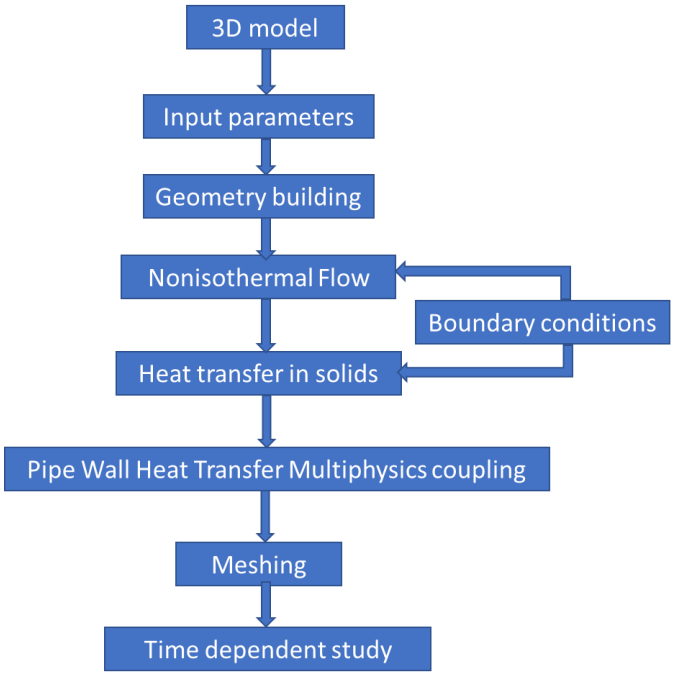


Figure 2. Flowchart illustrating the numerical modelling process of the closed-loop heat exchangers

2.2.1. Model assumption

To enable tractable analysis of fluid flow and heat transfer processes in CBHEs while isolating the effects of geometric configuration, the following assumptions were adopted:

(1) Heat transfer between the coaxial casing and the surrounding formation is assumed to occur exclusively through conduction. This isolates geometric effects from convective interactions within the formation and focuses the analysis on differences attributable to well configuration.

(2) The working fluid and the surrounding formation are assumed to reach local thermal equilibrium at each computational time step. The long operating cycle of geothermal systems relative to the circulation time of the fluid ensures adequate heat exchange.

(3) The thermo-physical properties of the formation, cement grout, and casing are treated as constant and temperature-independent.

(4) Seasonal variations in surface temperature are ignored, as they predominantly affect only the shallow subsurface. In high-temperature systems, these effects could be negligible relative to formation temperatures at depth.

2.2.2. Mathematical formulations

To resolve the fluid behaviour within the CBHE, the flow in all pipe segments is assumed to be fully developed. The numerical model solves one-dimensional governing equations for velocity, pressure, and temperature of a Newtonian fluid circulating through a closed-loop system embedded in a rock mass characterised by geothermal gradient-controlled temperatures. Water is selected as the working fluid, using COMSOL's in-built thermo-physical properties. The fluid momentum and mass conservation equations are:

$$\rho_f \frac{\partial u}{\partial t} + \rho_f \mathrm{u} \cdot \nabla u = -\nabla p - f_D \frac{\rho_f}{2D} \mathrm{u}|\mathrm{u}| + \mathrm{F} \quad (1)$$

266

$$\frac{\partial A\rho_f}{\partial t} + \nabla\left(A\rho_f \mathrm{u}\right) = 0 \quad (2)$$

267

268 where ρ_f is the fluid density (kgm^{-3}), u is the tangential, cross-section averaged fluid velocity
269 (ms^{-1}), t the time (s), P the pressure (Pa), f_D the Darcy-Weisbach (D-W) friction factor
270 (dimensionless), F the gravitational volume force (Nm^{-3}), D and A are the borehole inner
271 diameter (m) and the cross-section area (m^2). Taking into consideration the pressure losses
272 along the wellbore resulting from viscous shear, we utilize the (Haaland, 1983) [54] equation
273 to address the Darcy-Weisbach friction factor:

$$f_D = \left\{-1.8log\left[\frac{6.9}{Re} + \left(\frac{\varepsilon/D}{3.7}\right)^{1.11}\right]\right\}^{-2} \quad (3)$$

274 where the Reynold number Re = (ρ_f u D)/μ_f, μf is the fluid dynamic viscosity (Pa s) and ε (m)
275 is the surface roughness of pipe wall. The heat transfer radially at the interface between the
276 wall and fluid is expressed as follows:

$$Q_w = 2\pi hD(T_r - T_f) \quad (4)$$

277 Where Q_w is a source/sink term (Wm^{-1}) expressed for the radial heat exchange between the
278 fluid and rocks, T_{ext} (K) is the external temperature outside the pipe; h (Wm^{-2}K^{-1}) is the heat
279 transfer coefficient, which depends on the thermal conductivity of the borehole material λ_b, the
280 borehole inner diameter (D) and Nusselt number (N_u) that refers to the physical properties of
281 the fluid and the nature of the flow:

$$h = N_u \frac{\lambda_b}{D} \tag{5}$$

where Nu for turbulent flow is expressed as follows (GNIELINSKI, 1976) [55]:

$$N_u = \frac{(f_D/8)(\mathrm{R_e} - 1000)\mathrm{P_r}}{1 + 12.7(f_D/8)^{1/2}(\mathrm{P_r}^{2/3} - 1)} \tag{6}$$

Where Prandtl number is $\mathrm{P_r} = (C_p \mu)_f/\lambda_f$. Equation 3.10 is valid for $0.5 \leq \mathrm{P_r} \leq 2000$ and $3000 \leq \mathrm{R_e} \leq 5 \cdot 106$.

Within this module, the physics interfaces establish the conservation of momentum, energy, and mass for fluid within a pipe or channel. The flow rate, pressure, temperature, and concentration fields are represented as averages across the cross-section, exhibiting variation solely along the pipe's length.

2.2.3. Initial and boundary conditions

The numerical investigation considers a coaxial closed-loop geothermal system applied to Vulcano, a volcanic island of the Aeolian Archipelago located in the southern Tyrrhenian Sea (Italy). Initial and boundary conditions follow those defined in Mohaman et al. (2025) [48]. The initial temperature field corresponds to the undisturbed geothermal gradient, while far-field boundaries are held at constant temperature. At the well inlet, the fluid temperature (T_in, ^{0}C) and volumetric flow rate (q_v, Ls^{-1}) were imposed. The outlet boundary was treated as open, subject to two-point constraints for heat and mass transport. Outlet pressure was maintained at P>1 bar to avoid phase change at high temperature (Gola et al., 2022) [56]. Coupling between pipe flow and solid heat transfer enabled simulation of subsurface wellbore thermal interactions throughout the system’s operational lifespan. A steady-state simulation was first performed to obtain the undisturbed formation temperature field; this served as the

initial condition for subsequent transient simulations. All simulations assume continuous operation over a 25-year period to assess long-term thermal sustainability.

2.3.Meshing and Solutions

Based on the thermo-physical parameters of the Vulcano geological settings, this study utilized COMSOL Multiphysics software to construct one-dimensional physical models of three geothermal systems. Fully coupled approach is employed to solve the model. The discrete time step was set as 1 d. The absolute tolerance is regarded as the convergence criterion and set to 10^{-5}. Mesh generation is performed to achieve the spatial discretisation of the model in Figure 3(a-c). It is seen that the 1D wellbore and 3D formation produce a complete geometric model. Mesh independence analysis is also performed to reduce the discrete error. Physics-controlled and user-controlled mesh sizes were generated for the CBHE domain and the surrounding rock-soil domain. mesh configurations ranging from coarse to fine were tested, with predefined minimum and maximum user-controlled mesh sizes. All tested mesh configurations produced comparable results with only minor differences after 10000 days of simulation, as shown in Table 4-8. In this study and considering both computational efficiency and accuracy, the user-controlled mesh was selected for the V-CBHE, D-CBHE, H-CBHE, U-CBHE and SL-CBHE models as it provided results with the minimum element quality while optimizing computational time.

Table 4. Sensitivity analysis for V-CBHE mesh selection

Mesh size	Number of domain elements	Number of boundary elements	Number of edge elements	Minimum element quality	Production temperature at t = 10000 days (°C)
Coarse	2261	888	179	0.28650	109.23
Normal	6675	1702	248	0.24970	104.41
Fine	14249	2784	318	0.22510	104.03
Finer	40888	4930	430	0.22580	101.93
User defined 1	337881	9196	1820	0.15990	95.98
User defined 2	465508	15240	2024	0.16970	95.98
User defined 3	1878131	51130	2696	0.16540	95.96

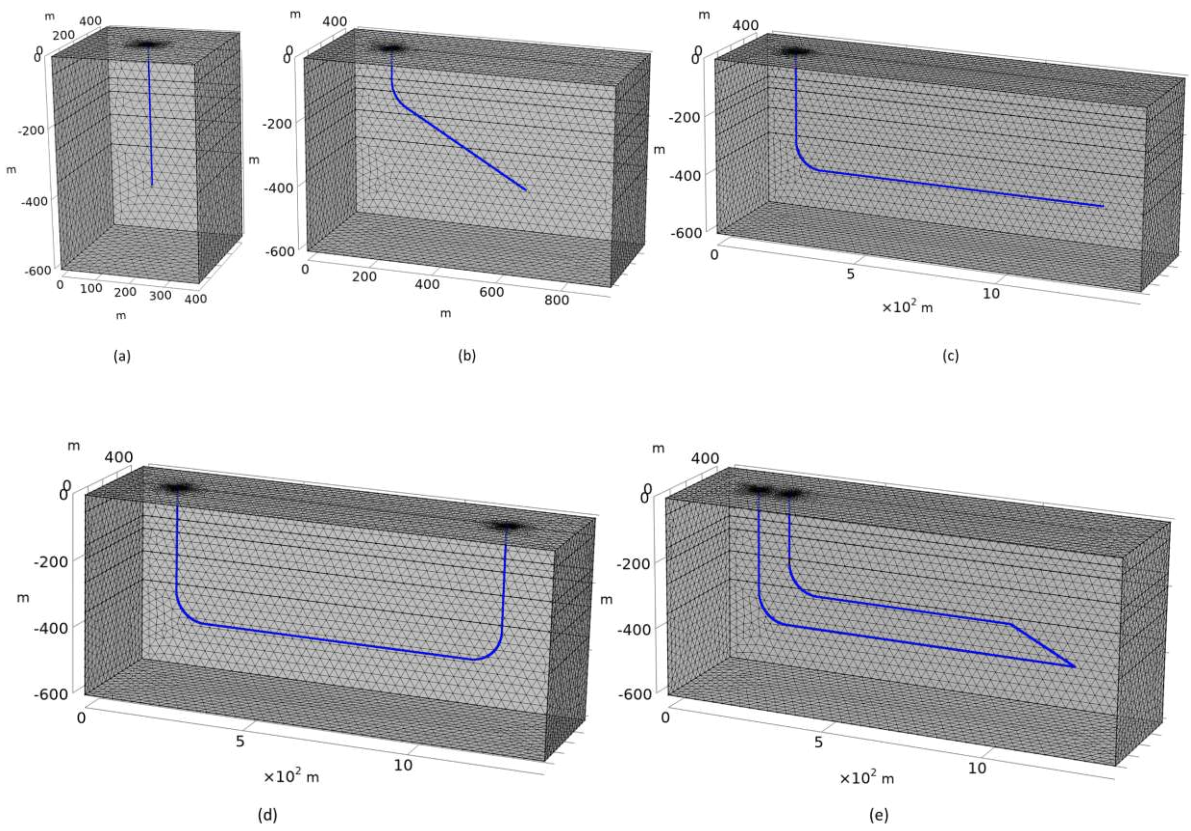


Figure 3. Numerical meshing schemes: (a) V-CBHE; (b) D-CBHE; (c) H-CBHE; (d) U-CBHE and (e) SL-CBHE

325 **Table 5.** Sensitivity analysis for D-CBHE mesh selection

Mesh size	Number of domain elements	Number of boundary elements	Number of edge elements	Minimum element quality	Production temperature at t = 10000 days (◦C)
Coarse	2040	920	199	0.12570	137.94
Normal	4665	1596	261	0.19830	129.25
Fine	8555	4837	329	0.11160	122.09
Finer	23437	4204	433	0.19370	119.01
User defined 1	562351	15054	2863	0.17880	102.22
User defined 2	892589	28966	3207	0.17870	102.21
User defined 3	4254451	102262	4257	0.18870	102.19

326

327 **Table 6.** Sensitivity analysis for H-CBHE mesh selection

Mesh size	Number of domain elements	Number of boundary elements	Number of edge elements	Minimum element quality	Production temperature at t = 10000 days (◦C)
Coarse	2684	1012	197	0.16680	197.38
Normal	7403	1920	280	0.21490	189.67
Fine	14516	3090	362	0.26580	179.83
Finer	45878	5808	498	0.23010	172.03
User defined 1	545369	12352	2788	0.16050	135.59
User defined 2	780578	22578	3076	0.19510	135.61
User defined 3	3217439	78318	3944	0.16180	135.54

328

329 **Table 7.** Sensitivity analysis for U-CBHE mesh selection

Mesh size	Number of domain elements	Number of boundary elements	Number of edge elements	Minimum element quality	Production temperature at t = 10000 days (◦C)
User defined 1	1153450	10232	6124	0.11589	150.90
User defined 2	1204942	10535	6143	0.13680	150.51
User defined 3	1195780	11360	6190	0.18310	150.56
User defined 4	1224796	13286	6302	0.16350	150.47
User defined 5	1356646	22940	6692	0.18830	150.47
User defined 6	1829868	41374	7134	0.17530	150.46
User defined 7	6774141	145712	8506	0.18430	150.40

330

331 **Table 8.** Sensitivity analysis for SL-CBHE mesh selection

Mesh size	Number of domain elements	Number of boundary elements	Number of edge elements	Minimum element quality	Production temperature at t = 10000 days (◦C)
User defined 1	1730850	10985	8929	0.17410	164.94
User defined 2	1750645	11744	8969	0.16360	164.90
User defined 3	1763524	13290	9047	0.17910	164.88
User defined 4	1803581	16168	9193	0.17260	164.87
User defined 5	1900283	22902	9437	0.17860	164.86
User defined 6	2371466	41644	9879	0.17510	164.86
User defined 7	7293426	145748	11251	0.17150	164.85

332

333 2.4.Model validation

334 This study provides a preliminary feasibility assessment of coaxial closed-loop borehole heat
335 exchangers (CBHEs) on Vulcano Island (Aeolian Archipelago). As no CBHE installations
336 currently exist on the island, site-specific data are unavailable for direct validation.
337 Consequently, model validation is performed by evaluating the capability of the numerical
338 framework to reproduce the general thermal behaviour of CBHE systems. Consistent with the

approach adopted in Mohaman et al. (2025) [48], the model was validated against field-test data from Huajun et al. (2016) [57]. Table 9 and 10 shows the geometric and material parameters.

Table 9. Thermophysical properties of rock samples in different layers (L1–L4).

Layer	Value (m)	λ [W/(m·K)]	ρ [kg/m³]	Cp [J/(kg·K)]	Porosity (%)
Layer 1	0-300	1.75	1980	1350	36.1
Layer 2	300-1020	2.05	2050	1050	25.2
Layer 3	1020-1200	4.10	2680	845	6.6
Layer 4	1200-1800	5.35	2850	860	0.7

Table 10. Parameters of DBHE on site.

Parameter	Value
Outer pipe, mm	177.8
Outer pipe thickness, mm	8.05
Inner pipe, mm	100.9
Inner pipe thickness, mm	10.45
Depth of deep CBHE, m	1800
Outer pipe λs, W/(m·K)	44
Outer pipe λ, W/(m·K)	0.4

To model the working fluid, the average measured injection temperature is implemented in this study to serve as the boundary condition at the inlet of the deep CBHE. The ground temperature almost increased linearly with depth, Z (Huajun et al., 2016) [57], and can be expressed by Eq. (17).

$$T = 14.30924 + 0.02477Z \quad (7)$$

where the units of T and Z are ^{0}C and m, respectively. Model accuracy was evaluated using RMSE and MAPE, which quantify absolute error and percentage deviation, respectively (Armstrong et al., 1992; Kim et al., 2016) [58,59]. The formulas for these metrics are provided in Kim et al., 2016; Caulk et al., 2017 [59,60] as follows:

$$\mathrm{MAPE} = \frac{1}{n}\sum_{i=1}^{n}\frac{|T_m - T_s|}{T_a} \quad (8)$$

$$\mathrm{RMSE} = \frac{1}{n}\sum_{i=1}^{n}\left|T_m - T_s\right| \quad (9)$$

with T_m as the field-measured temperature (^{o}C) and T_s as the simulated value across n temperature data points.

Figure 4(a) compares the simulated outlet temperature with field measurements for a flow rate of 20.03 m³/h over a 46-hour operational period, during which the average inlet temperature was 11.24 °C. Similar numerical simulation trend as the 2D-axisymetric model in Mohaman et al. (2025) [48] is observed. In addition, the simulated outlet temperatures are slightly higher than the measured values, particularly during the initial phase of operation. As reported in Mohaman et al. (2025) [48], this discrepancy is likely attributable to limitations in transient simulations when capturing the dynamic onset of fluid circulation, a phenomenon also noted by Huajun et al. (2016) [57]. Additional contributing factors include the use of an averaged inlet temperature and the adopted mesh configuration.

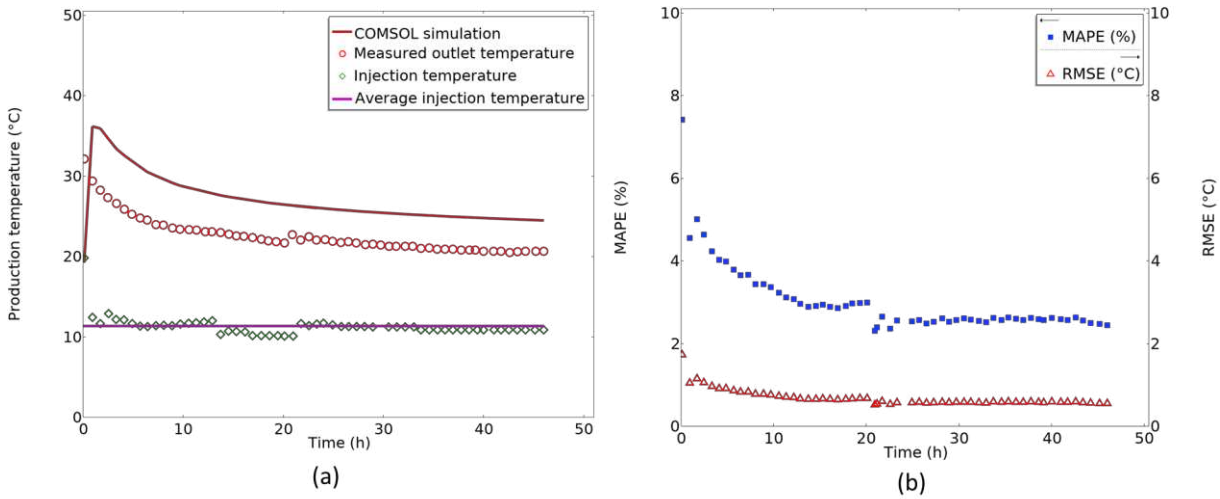


Figure 4. (a) Modified 1D-3D model and Huajun et al., 2022 field and modelling results comparison, and (b) MAPE (%) and MAE (^{0}C)

Furthermore, the calculation result of the numerical model is slightly higher than the measured data outlet temperature. The error is explained as follows:

(1) The actual formation parameters (geothermal gradient, physical parameters of the rock, etc.) are very complex. These parameters have been simplified during modelling.

(2) The flow of groundwater is not considered, which will cause the calculation result to be higher than the actual situation.

(3) During modelling, it is assumed that the casing and cement sheath as well as the cement sheath and the formation are in perfect contact. However, there may be loose contact in the actual construction, which will lead to high calculation results.

(4) The inlet temperature in the field experiment was not always maintained at 11.24 °C.

Moreover, as discussed in Mohaman et al. (2025) [48], Figure 4(b) presents the temporal evolution of model accuracy in terms of MAPE and RMSE. The MAPE remained below 5% throughout the simulation period, while the RMSE stabilized at approximately 0.5 °C after the initial transient phase. These results confirm the reliability and accuracy of the numerical model

and demonstrate the robustness of the coupled 1D–3D heat transfer framework for vertical well configurations.

Although direct validation using measured data is not available for the D-CBHE, H-CBHE, U-CBHE, and SL-CBHE configurations, it is reasonable to extend the applicability of the validated model to these systems (Wang et al., 2021) [14]. This inference is justified by the consistent use of modelling assumptions, meshing strategies, governing equations, and numerical solution methods across all CBHE configurations considered in this study.

2.5.Energy Estimation

Evaluating the geothermal energy potential of the analysed closed-loop geothermal systems requires careful assessment of the outlet temperatures predicted by the numerical simulations. System performance is evaluated primarily in terms of long-term production temperature and thermal power extraction.

$$P_{th} = q_v \cdot \rho \cdot C_p \cdot (T_{prod} - T_{in}) \quad (10)$$

Where P_{th} is the extracted thermal power (kW_{th}), q_v is the volumetric flow rate of the fluid (Ls^{-1}), ρ is the density of the fluid ($kg\ m^{-3}$), C_p is the specific heat capacity of the fluid, calculated at the medium temperature between T_{prod} and T_{in} ($J\ kg^{-1}\ K^{-1}$), T_{prod} is the production temperature of the geothermal fluid coming out from the well ^0C, T_{in} is the inlet temperature of the fluid reinjected into the well (^0C).

Electrical power estimate is derived using simplified binary-cycle correlation (Eq 11) as reported in Mohaman et al. (2025) [48] and is interpreted strictly as comparative indicator.

$$P_e = P_{th} \cdot [6.9681 \times Ln(T_{prod}) - 29.713] \quad (11)$$

Absolute power values are not intended as production forecasts; instead, emphasis is placed on relative performance ranking among different borehole geometries.

3. Results and Discussion

3.1. Heat extraction of CBHE configurations

This section presents the long-term thermal behaviour of vertical (V-CBHE), deviated (D-CBHE), horizontal (H-CBHE), U-loop (U-CBHE) and single-lateral (SL-CBHE) closed-loop borehole heat exchangers and the comparison between them under identical geological and operational conditions. First operational and geometric parameters sensitivity analysis have been conducted with respect to production temperature, with both operational and geometric parameters sensitivity on D-CBHE and H-CBHE. The comparison has been focused on thermal interaction with the surrounding formation and the resulting energy performance of the different configurations.

3.1.1. V-CBHE

Figure 5a illustrates the locations of control line (CL) points at depths of 50, 200, 300 m, and at the bottom hole, used to evaluate thermal interaction between the wellbore and the surrounding formation. Figure 5b presents the working-fluid temperature evolution along the vertical coaxial borehole heat exchanger (V-CBHE) after one year of continuous operation. The temperature profile reflects the coupled effects of advective heat transport within the coaxial pipes and conductive heat exchange with the surrounding geological formation. Along the downward flow path, the injected fluid undergoes a gradual temperature decline due to heat losses to the cooler shallow subsurface. With increasing depth, the temperature gradient decreases as formation temperatures rise and radial heat flux is reduced, reaching a bottom-

hole temperature of approximately 100 °C. During upward flow in the annular section, partial temperature recovery occurs due to internal heat exchange between the downflow and upflow streams, resulting in an outlet temperature of about 98 °C. This internal thermal short-circuiting smooths the axial temperature profile and indicates that the system approaches a quasi-steady thermal regime after one year of operation.

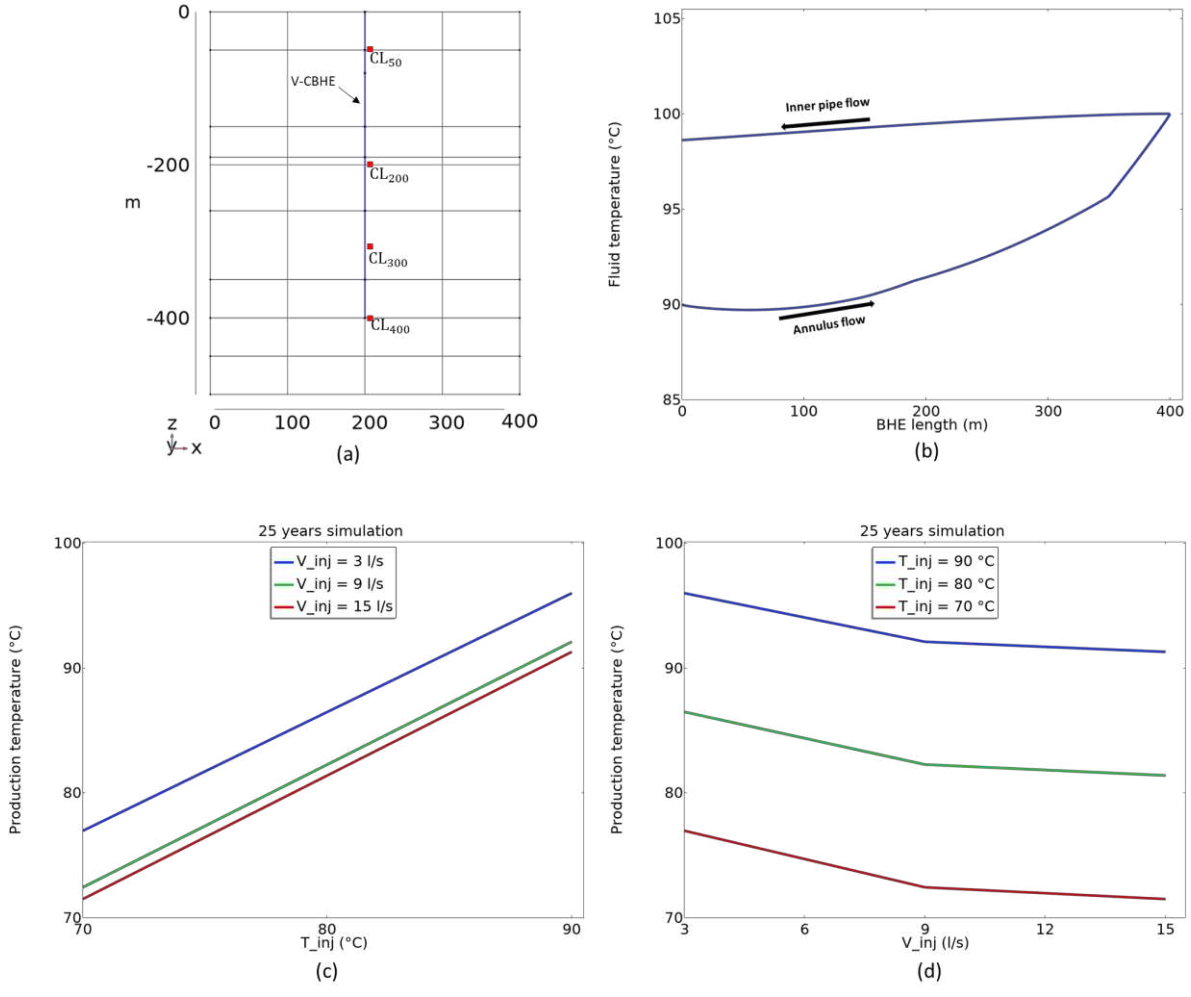


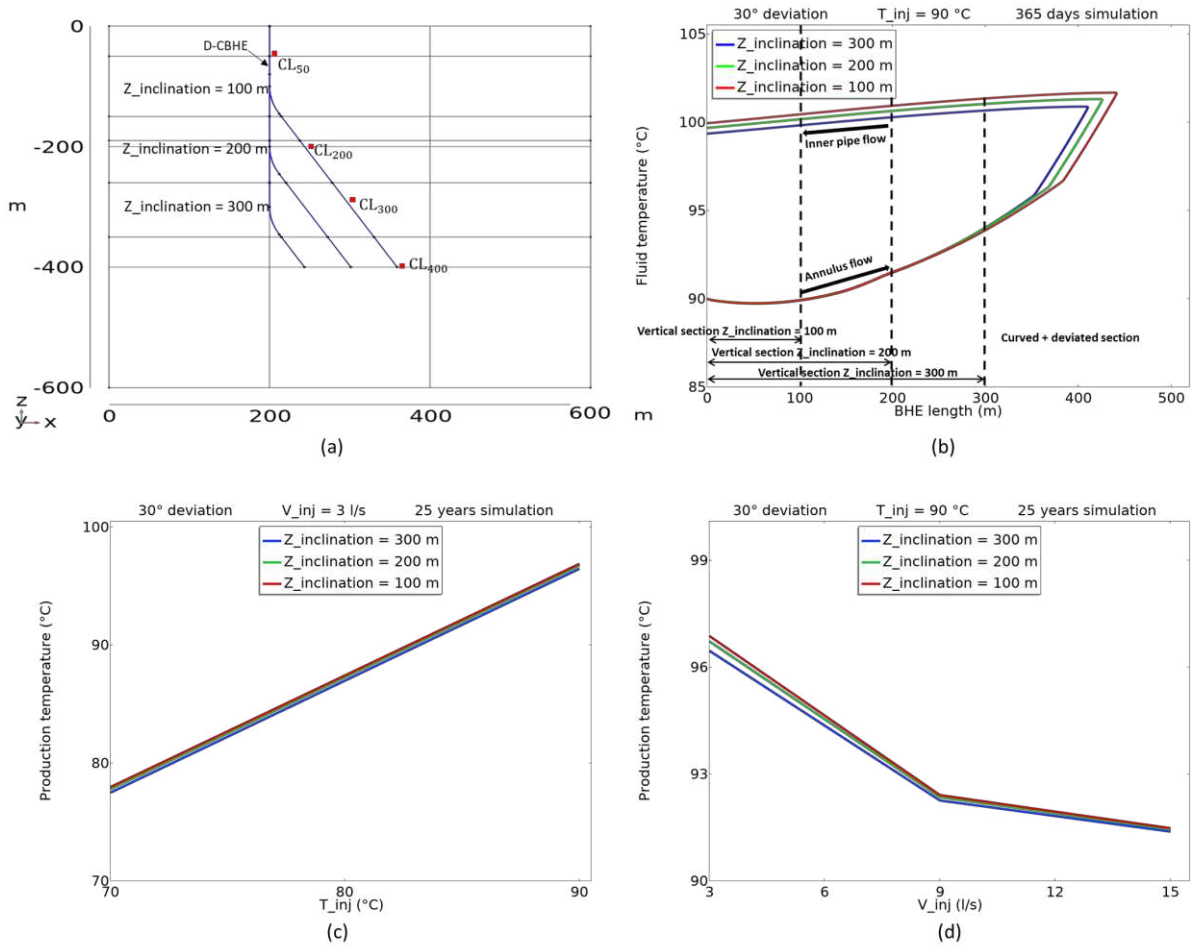
Figure 5. (a) V-CBHE and position of control points; (b) Heat carrier fluid temperature evolution along the V-CBHE after 1 year of continuous operation; (c) Effects of injection temperature and (d) Effects of injection flow rate on production temperature after 25 years of continuous operation.

Figures 5c and 5d show the sensitivity of long-term performance after 25 years of operation. Production temperature increases nearly linearly with injection temperature, with a 15–20 °C increase observed when T_inj rises from 70 to 90 °C. Conversely, higher injection flow rates

reduce outlet temperature due to shorter residence time and diminished conductive heat uptake. The intermediate flow rate of 9 L s^{-1} represents a balanced regime, optimising heat extraction through a trade-off between advective transport and conductive heat transfer.

3.1.2. D-CBHE

Figure 6a and Figure 7a shows the locations of control line (CL) points used to analyse thermal interaction along the deviated coaxial borehole heat exchanger (D-CBHE). Figure 6b presents the axial evolution of working-fluid temperature after one year of continuous operation for different deviation depths. The results indicate only a minor influence of deviation depth on thermal performance. Bottom-hole temperatures vary slightly from approximately 101.7 °C for a deviation depth of 100 m to 100.9 °C for 300 m, with corresponding outlet temperatures differing by less than 1 °C. This limited sensitivity reflects the modest increase in effective heat-exchange length achieved by altering deviation depth alone.



452

453 **Figure 6.** (a) D-CBHE different inclination depth and position of control points; (b) Heat carrier fluid temperature evolution
454 along the D-CBHE after 1 year of continuous operation; (c) Effects of injection temperature and (d) Effects of injection flow
455 rate on production temperature after 25 years of continuous operation.

456

457 The effect of deviation angle is more pronounced, as shown in Figure 7. Increasing the
458 deviation angle from 30° to 60° enhances exposure to warmer formations, leading to higher
459 bottom-hole temperatures of approximately 101 °C, 104 °C, and 110 °C, respectively, after one
460 year of operation. Corresponding outlet temperatures increase to about 99 °C, 101 °C, and 106
461 °C. After 25 years of operation (Figures 7c–d), production temperature increases nearly linearly
462 with injection temperature for all deviation angles, with the 60° configuration consistently
463 outperforming lower angles. Conversely, increasing injection flow rate reduces production

temperature due to shorter residence time. At flow rates above 9 L s^{-1}, outlet temperatures converge toward a convective-dominated regime, indicating diminishing thermal gains. Overall, while deviation angle improves performance relative to vertical systems, D-CBHEs remain limited by comparatively short residence times and restricted lateral heat-exchange area.

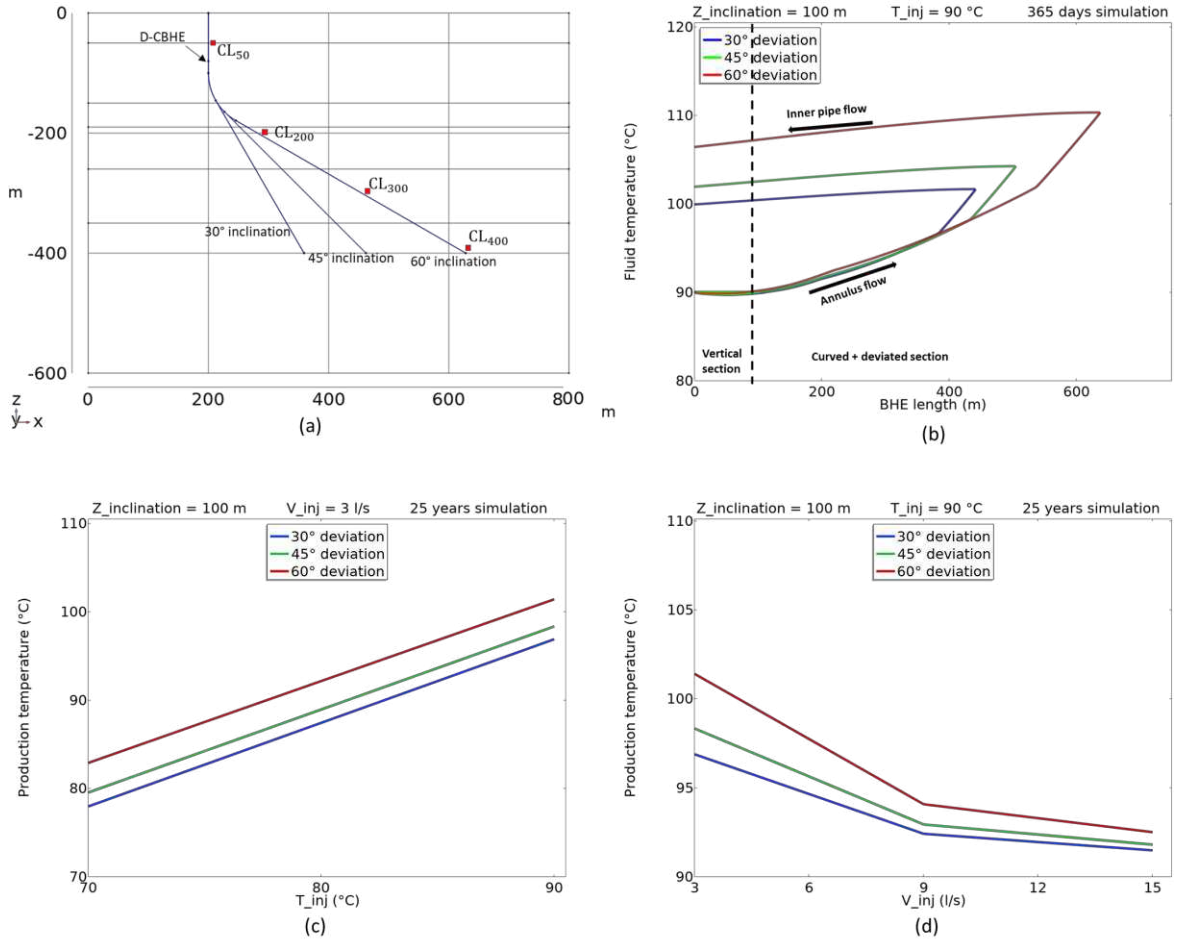


Figure 7. (a) D-CBHE different inclination angle and position of control points; (b) Heat carrier fluid temperature evolution along the D-CBHE after 1 year of continuous operation; (c) Effects of injection temperature and (d) Effects of injection flow rate on production temperature after 25 years of continuous operation.

3.1.3. H-CBHE

Figure 8a illustrates the geometry and CL locations for the horizontal coaxial borehole heat exchanger (H-CBHE). Figure 8b shows the working-fluid temperature evolution after one year of continuous operation for horizontal extensions (HL) ranging from 200 to 1000 m. In all cases, fluid temperature increases monotonically along the flow path, indicating sustained conductive heat uptake from the surrounding formation. Shorter horizontal lengths (200–400 m) yield outlet temperatures of approximately 119–133 °C, while longer laterals significantly enhance performance. For HL = 600, 800, and 1000 m, outlet temperatures increase to approximately 146 °C, 157 °C, and 167 °C, respectively, after one year.

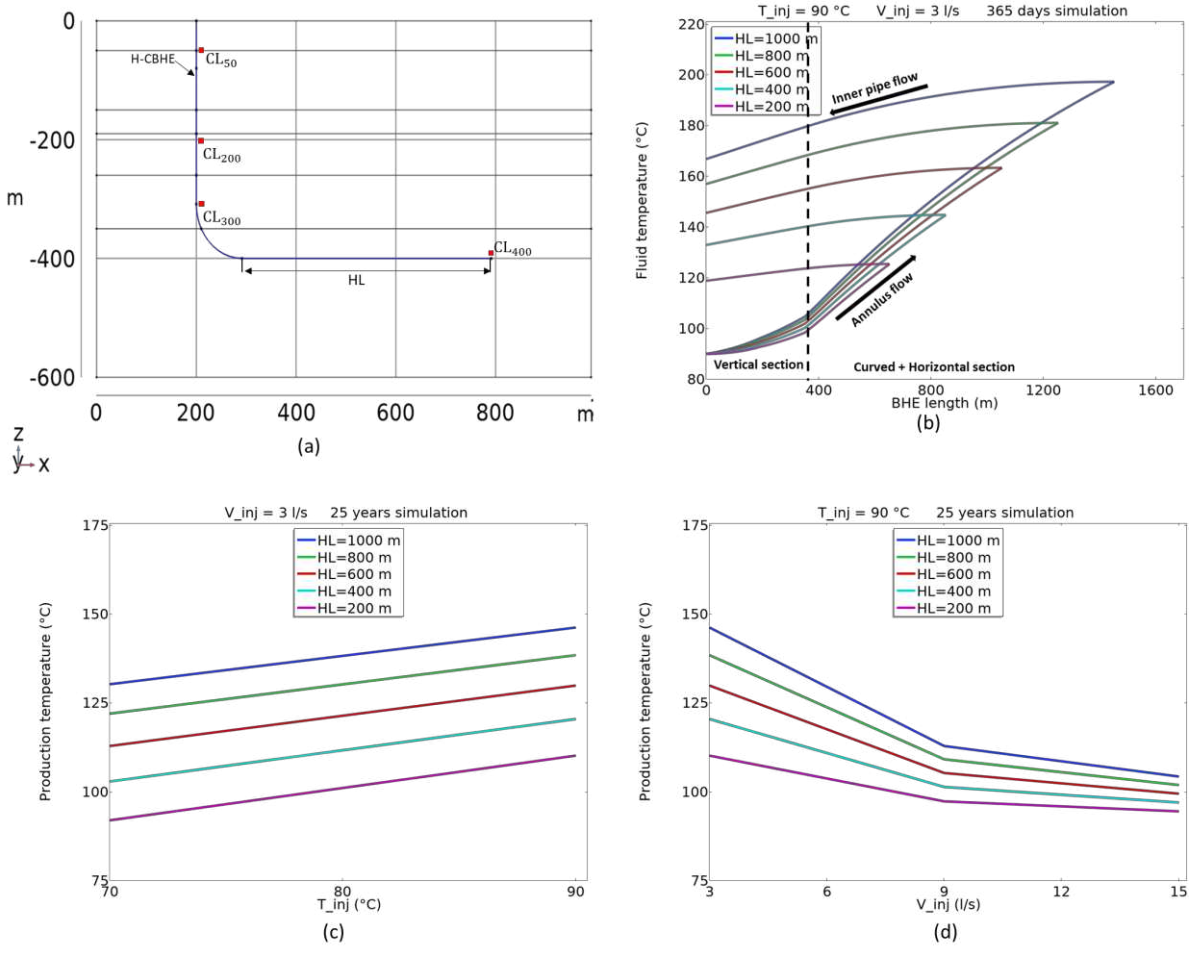
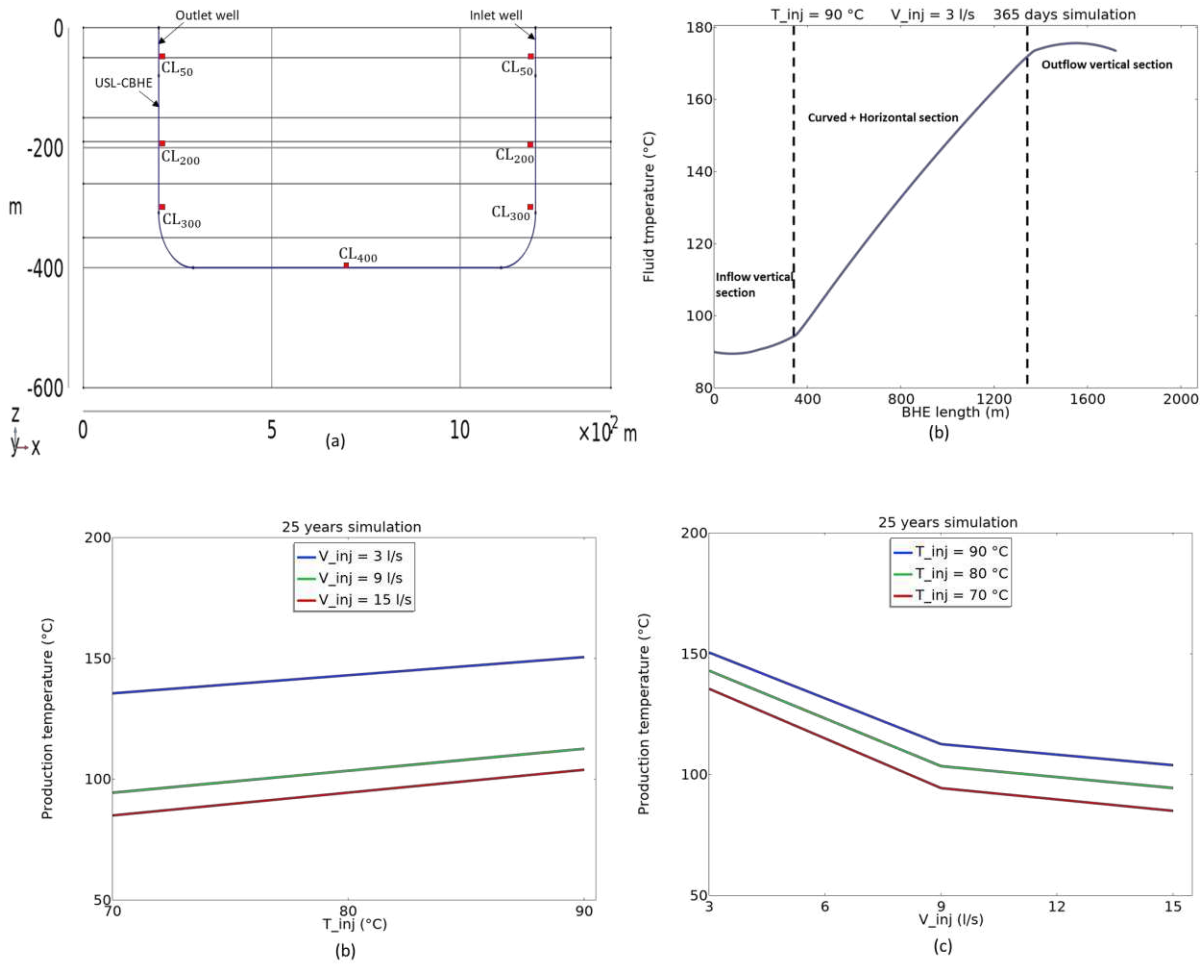


Figure 8. (a) H-CBHE and position of control points; (b) Heat carrier fluid temperature evolution along the H-CBHE after 1 year of continuous operation for each horizontal elongation; (c) Effects of horizontal elongation on production temperature for different injection temperature and (d) Effects of horizontal elongation on production temperature different injection flow rate, after 25 years of continuous operation.

Long-term results after 25 years (Figure 3.8c) show that production temperature increases almost linearly with horizontal length across all injection temperatures. At T_inj = 90 °C, outlet temperatures stabilise at approximately 110–130 °C for HL ≤ 600 m and increase to about 138 °C and 146 °C for HL = 800 m and 1000 m, respectively. Figure 3.8d demonstrates that increasing injection flow rate reduces outlet temperature for all configurations, particularly beyond 9 L s^{-1}, due to reduced residence time and accelerated thermal depletion near the borehole. Nevertheless, the relative performance ranking remains unchanged, confirming that extended horizontal sections effectively compensate for advective limitations. These results highlight horizontal elongation as one of the most effective geometric strategies for enhancing closed-loop geothermal performance in shallow, high-temperature volcanic environments.

3.1.4. U-CBHE

Figure 9a presents the geometry and CL locations for the U-CBHE. The working-fluid temperature evolution after one year of operation is shown in Figure 9b. Unlike purely coaxial systems, the temperature increase along the flow path is non-linear, reflecting variations in heat-exchange conditions along vertical, curved, and horizontal segments. The fluid temperature reaches a maximum of approximately 176 °C at about three-quarters of the total flow path, primarily within the horizontal lateral section. During upward flow toward the production wellhead, the fluid loses approximately 3 °C due to heat exchange with cooler shallow formations, resulting in an outlet temperature of about 173 °C.



508

509 **Figure 9.** (a) U-CBHE different inclination angle and position of control points; (b) Heat carrier fluid temperature evolution
510 along the U-CBHE after 1 year of continuous operation; (c) Effects of injection temperature and (d) Effects of injection flow
511 rate on production temperature after 25 years of continuous operation.

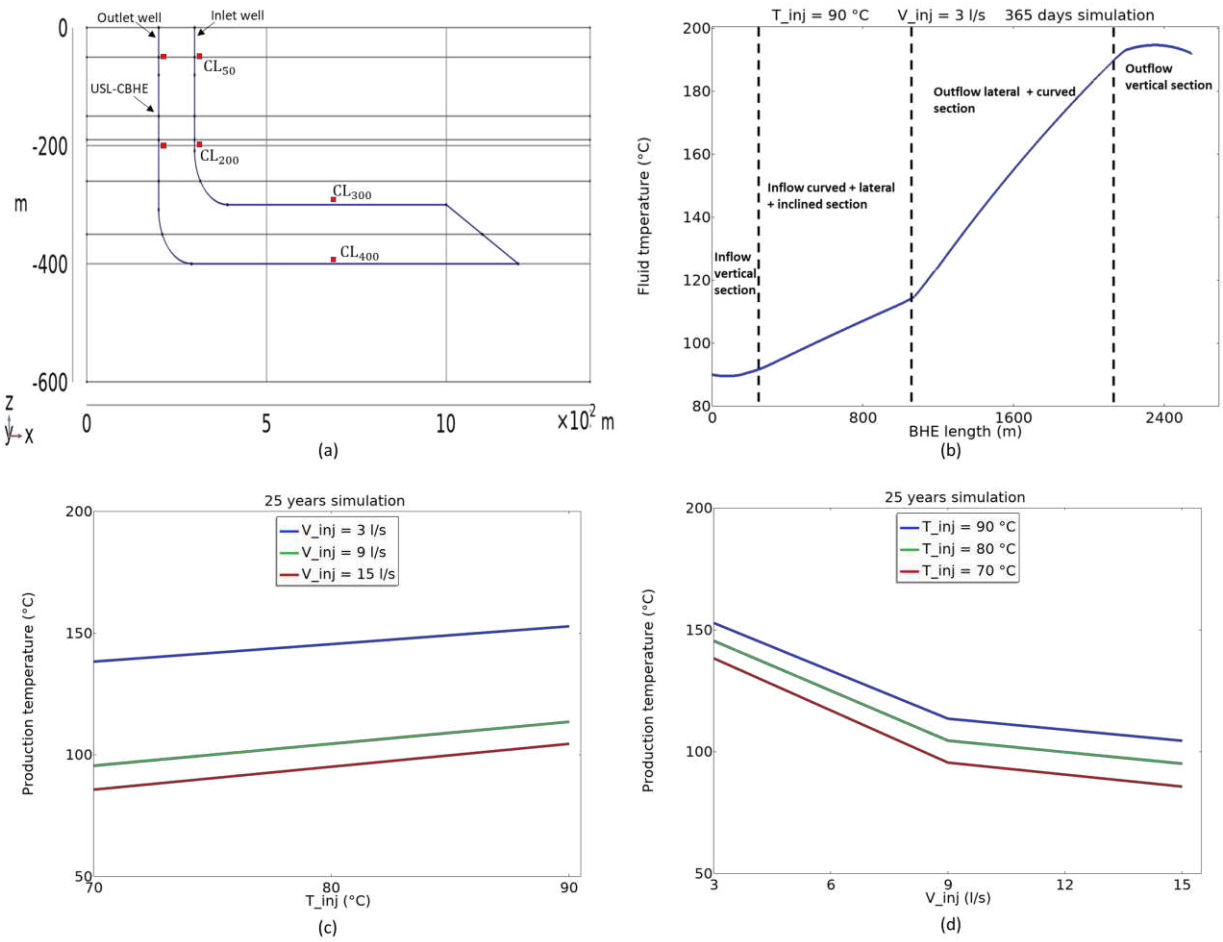
512

513 Figures 9c and 9d show the sensitivity of long-term performance after 25 years. Production
514 temperature increases linearly with injection temperature, confirming stable heat-transfer
515 efficiency over prolonged operation. Increasing the injection flow rate reduces outlet
516 temperature due to shorter residence time and diminished conductive heat uptake.
517 Nevertheless, even at moderate flow rates, the U-CBHE maintains high outlet temperatures
518 relative to coaxial-only configurations. Minimal thermal loss is observed along the vertical
519 ascent, indicating that most heat extraction occurs within the lateral section. These results

demonstrate that the U-CBHE efficiently combines vertical access with extended lateral exposure, enabling high and sustained production temperatures under shallow volcanic conditions.

3.1.5. SL-CBHE

Figure 10a shows the geometry and CL locations for the single-lateral closed-loop borehole heat exchanger (SL-CBHE). Figure 10b illustrates the axial temperature evolution after one year of continuous operation at an injection flow rate of 3 L s^{-1}. Following a minor initial temperature decrease near the injection point, the fluid temperature increases steadily along the curved and inclined segments, reaching approximately 124 °C before entering the lower lateral. Along this bottom lateral section, prolonged residence time and enhanced contact with high-temperature formations result in a pronounced temperature rise to about 193 °C. The outlet temperature stabilises near 191 °C, indicating limited thermal loss during ascent.



532

533 **Figure 10.** (a) SL-CBHE and position of control points; (b) Heat carrier fluid temperature evolution along the SL-CBHE after
534 1 year of continuous operation; (c) Effects of injection temperature and (d) Effects of injection flow rate on production
535 temperature after 25 years of continuous operation.

536 Long-term sensitivities after 25 years are shown in Figures 10c and 10d. At T_inj = 90 °C,
537 production temperatures reach approximately 165 °C, 119 °C, and 107 °C for injection flow
538 rates of 3, 9, and 15 L s^{-1}, respectively. Lower flow rates maximise outlet temperature by
539 increasing residence time, while higher flow rates reduce thermal equilibration despite
540 increased mass transport. The intermediate flow rate of 9 L s^{-1} represents a compromise
541 between heat uptake per unit mass and total heat extraction. Overall, the SL-CBHE exhibits
542 the highest long-term production temperatures among all configurations, demonstrating the
543 strong advantage of extended lateral exposure and multi-segment flow paths for closed-loop
544 geothermal systems in shallow volcanic settings.

3.2. Temperature distribution of the soil-rock formation

Figures 11 an12 respectively show the evolution of formation temperature fields gradient and radial temperature profiles at selected depths of 50 m, 200 m, 300 m and 400 m, over 10,000 days of operation. Clear differences emerge among the CBHE configurations. At shallow depths (50-200 m), all configurations exhibit limited thermal perturbation, approaching quasi-steady conditions relatively rapidly. The U-CBHE and SL-CBHE outlet wells shows elevated formation temperatures in the upper section, indicating heat losses to the shallower and cooler surrounding rocks, this could be mitigated through insulation the corresponding production pipe sections to a depth where thermal equilibrium is observed between the subsurface and the heat carrier fluid in the heat exchanger.

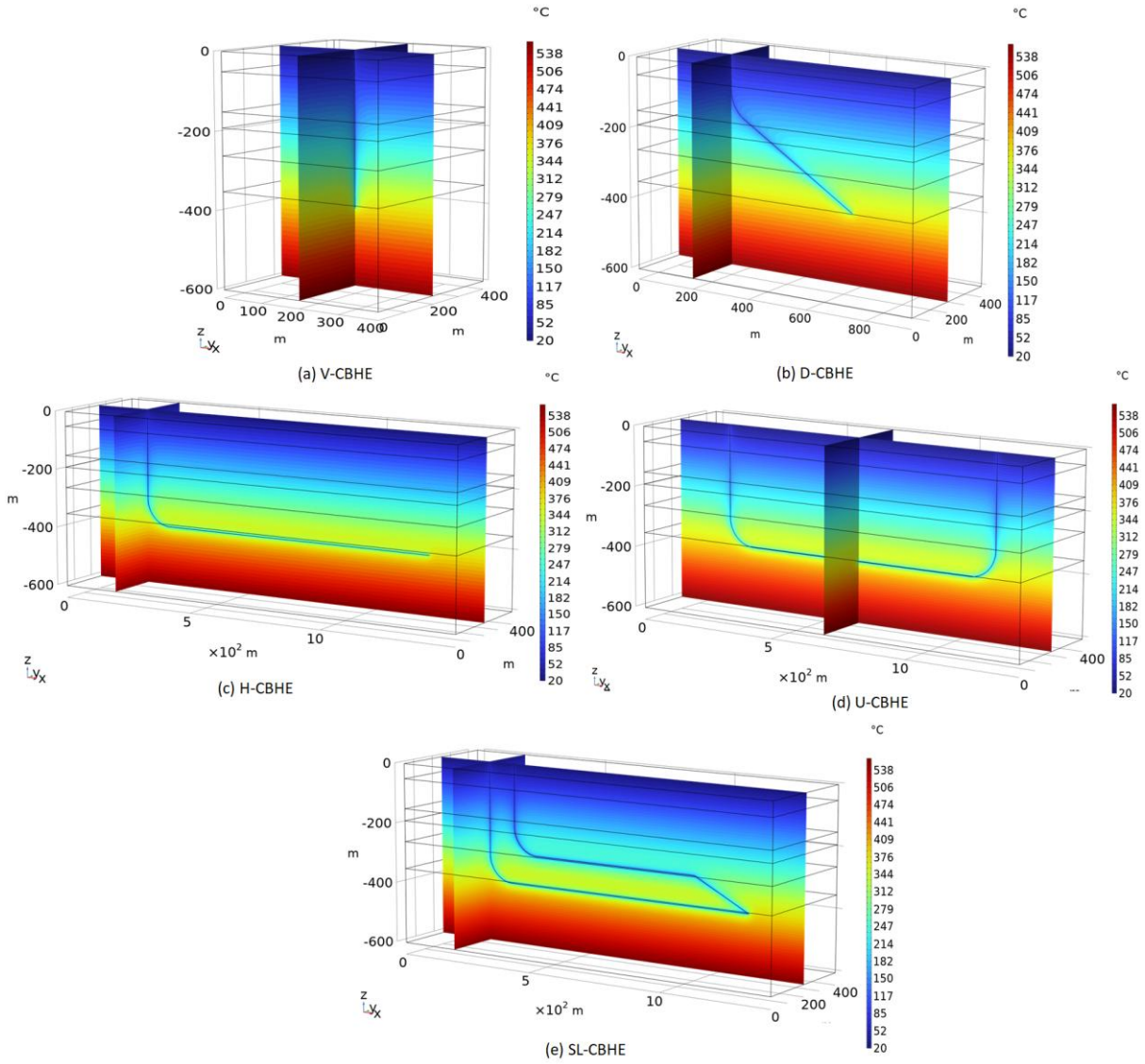


Figure 11. Formation temperature distribution of: (a) V-CBHE; (b) D-CBHE; (c) H-CBHE; (d) U-CBHE and (e) SL-CBHE.

At greater depths (300-400 m), geometric effects become more pronounced. The V-CBHE and D-CBHE produce more localized cooling near the borehole, reflecting limited thermal contact with high-temperature formations. In contrast, the H-CBHE U-CBHE and SL-CBHE induce broader but less concentrated thermal drawdown, distributing heat extraction over a larger rock volume. This spatial redistribution of thermal depletion delays localized temperature exhaustion, although it also produces a wider thermal footprint. These results suggest that lateral configurations improve long-term thermal utilisation by accessing a larger effective reservoir volume, rather than increasing instantaneous heat flux alone.

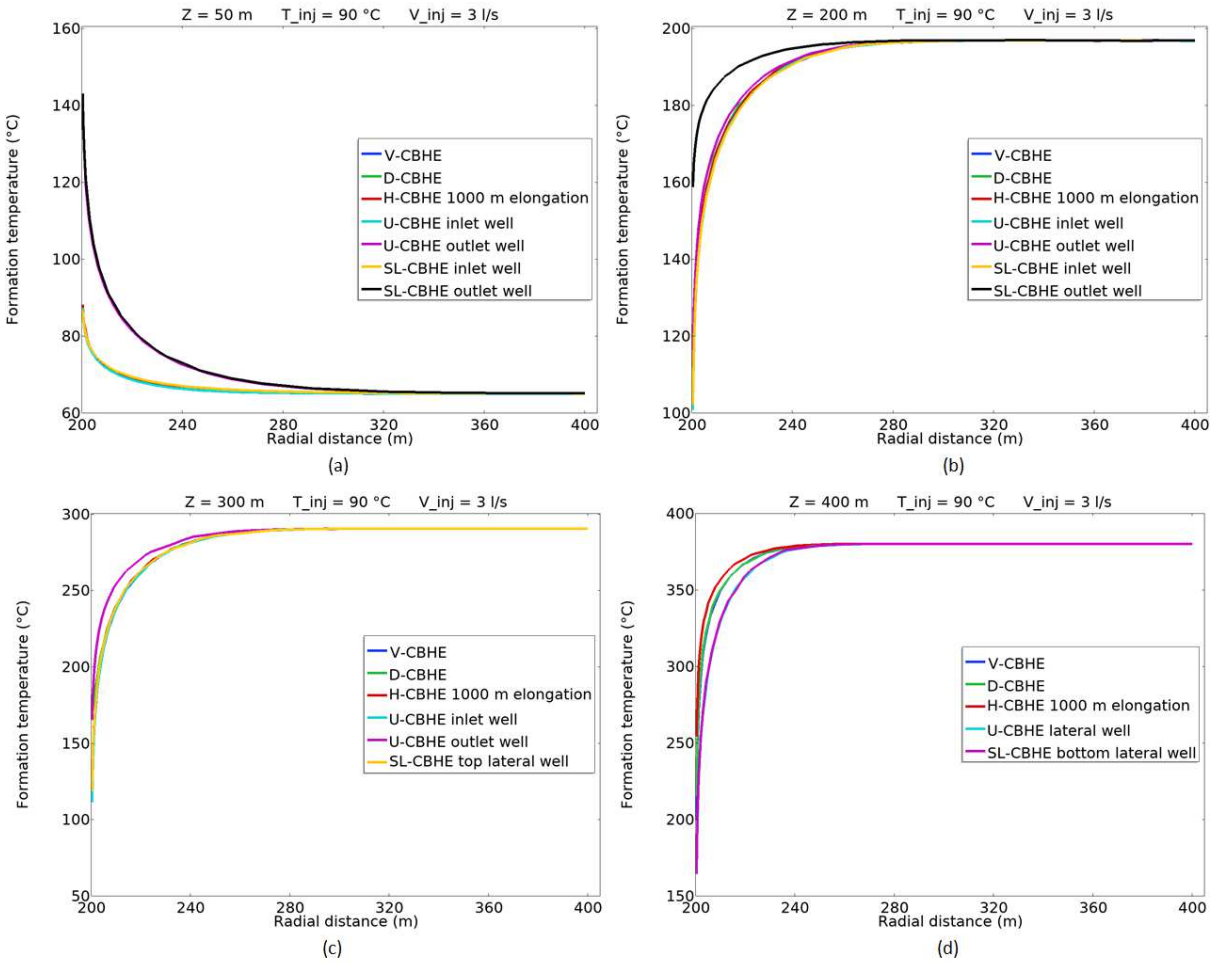


Figure 12. Comparison of time dependent formation temperature variation at 1 m radial distance control point from of the four borehole types, at: (a) 50 m; (b) 200 m; (c) 300 m and (d) 400 m depth during the system operation (90 °C injection temperature and 3 l/s injection flow rate).

3.3. Comparison of energy performance

Figure 13 compares the 25-year evolution of production temperature and the corresponding theoretical electrical power potential for the four CBHE configurations. The H-CBHE (1000 m horizontal section) and SL-CBHE exhibit the highest initial and long-term production temperatures, stabilising at approximately 147–165 °C after 25 years. These values correspond to estimated electrical power potentials of 8.6–11.9 MWe under idealised binary conversion assumptions. In contrast, the V-CBHE and D-CBHE stabilise at significantly lower temperatures (96-101 °C), resulting in substantially reduced electrical potential (0.8-1.6 MWe).

The rapid early decline observed for all configurations reflects the establishment of a cooled zone around the borehole; however, elongated and lateral systems maintain higher quasi-steady temperatures due to enhanced access to hotter formations and increased heat-exchange length.

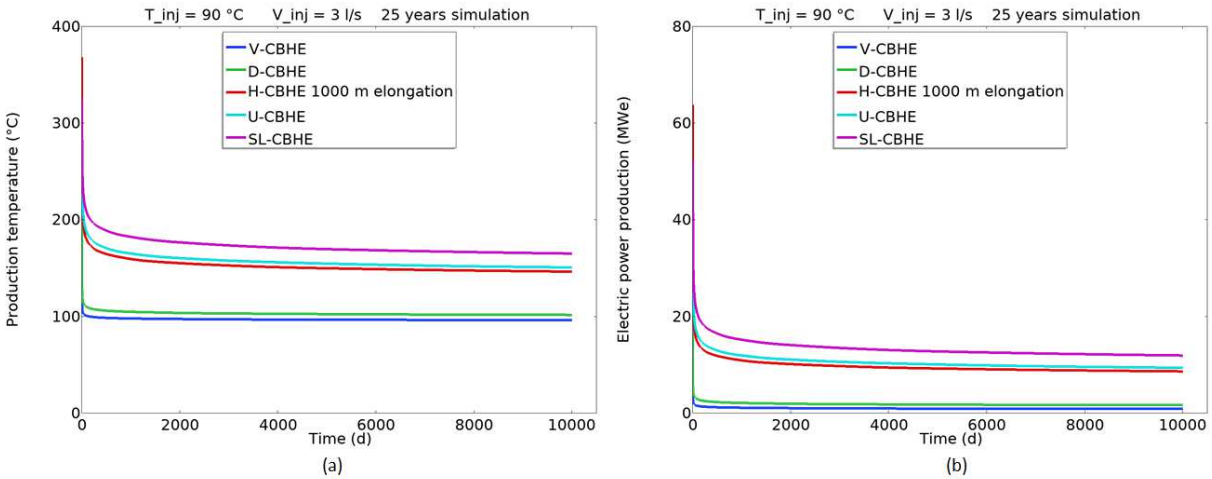


Figure 13. Comparison of (a) production temperature and (b) electric power production of the four close loop heat exchanger types.

It is important to note that these electrical power estimates represent theoretical upper bounds, as they neglect parasitic pumping losses, surface heat losses, and plant-specific operational constraints. Nevertheless, the relative performance ranking among configurations remains robust, underscoring the dominant role of borehole geometry in closed-loop geothermal system design.

3.4. Insulation effects

The insulation analysis evaluates the impact of different insulation strategies on the thermal performance of four closed-loop borehole heat exchanger (CBHE) configurations: vertical (V-CBHE), deviated (D-CBHE), horizontal (H-CBHE), and single-lateral (SL-CBHE). Performance is assessed through the working fluid temperature evolution along the borehole, which directly reflects heat extraction efficiency and thermal losses. As adopted in Mohaman et al. (2025) [38], for the coaxial configuration, full inner pipe (IP) insulation is simulated by

reducing its thermal conductivity from 0.18 W m^{-1} K^{-1} (polyethylene) to 0.05 W m^{-1} K^{-1}, representing a vacuum-insulated tubing (VIT). Outer pipe (OP) insulation depth is defined based on the depth at which the surrounding formation reaches thermal equilibrium with the injected fluid. In the insulated OP section, grout thermal conductivity is reduced from 1.5 to 0.05 W m^{-1} K^{-1} (expanded polystyrene equivalent). Scenarios range from no insulation to IP-only, OP-only, and combined IP&OP insulation, with OP insulation depths varying from 100 to 300 m. Results assess performance after one year of continuous operation at 90 °C injection temperature and 3 L s^{-1} flow rate.

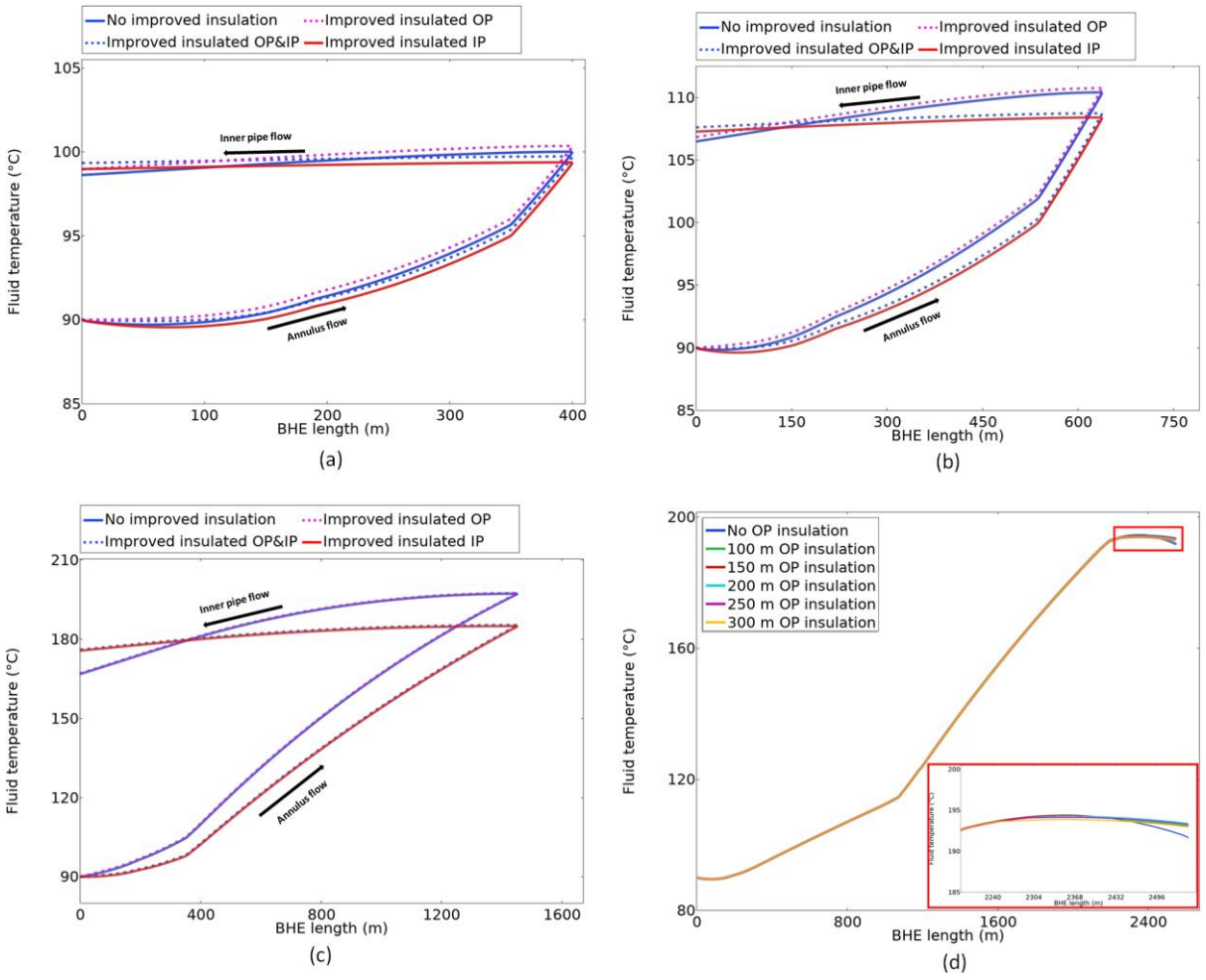


Figure 14. Effects on insulation on: (a) V-CBHE; (b) D-CBHE; (c) H-CBHE and (d) SL-CBHE.

Figure 14 (a–c) compares vertical (V-CBHE), deviated (D-CBHE), and horizontal (H-CBHE) coaxial closed-loop borehole heat exchangers, highlighting the influence of insulation strategies on the axial evolution of working-fluid temperature. In all cases, temperature trends reflect cumulative heat exchange with the surrounding formation, with stronger variations occurring in deeper or laterally extended sections. For the V-CBHE, outer pipe (OP) insulation provides only marginal improvement over the non-insulated case, as external heat transfer is dominated by boundary conditions and limited annular residence time, whereas inner pipe (IP) insulation yields a clearer performance enhancement by effectively reducing thermal short-circuiting between the downflow and up flow streams. The combined OP&IP configuration results in the highest outlet temperatures, although gains beyond IP-only insulation are modest, indicating diminishing returns once internal interference is minimized. Similar behaviour is observed for the D-CBHE, but with increased sensitivity to insulation due to the longer flow path and greater interaction with deeper, thermally stable formations, where IP insulation remains the dominant contributor. The H-CBHE exhibits the strongest insulation effects, particularly toward the exchanger end, where longer residence times and conduction-dominated heat transfer amplify internal losses; here, OP&IP insulation provides the most favourable temperature evolution. Figure 14d shows that increasing OP insulation depth progressively reduces thermal losses along the return leg of the SL-CBHE, with most benefits achieved within the upper 200 m, beyond which additional insulation yields diminishing gains. Overall, insulation effects are time-dependent and most pronounced during early operation, while long-term performance is primarily governed by mitigation of internal thermal short-circuiting through IP insulation across all coaxial CBHE systems.

4. Conclusion

This study provides a systematic numerical comparison of five closed-loop borehole heat exchanger (CBHE) configurations vertical coaxial, deviated coaxial, horizontal coaxial, U-loop and single-lateral operating under shallow, high-temperature volcanic conditions representative of Mediterranean island settings such as Vulcano Island (Italy). A validated coupled 1D wellbore–3D formation model was used to assess long-term thermal behaviour and energy performance over 25 years of continuous operation. The results demonstrate that:

- Borehole geometry and trajectory dominate system performance, outweighing the influence of operational parameters such as injection temperature and flow rate. Vertical and deviated CBHEs stabilise at relatively low production temperatures of approximately 96–101 °C after 25 years, reflecting limited thermal contact with high-temperature formations. In contrast, lateral configurations significantly enhance heat extraction by extending residence time within hotter subsurface layers. Horizontal coaxial, U-single-lateral, and single-lateral systems stabilise at substantially higher production temperatures of approximately 147–165 °C, corresponding to idealised electrical power potentials of 8.6–11.9 MWe, compared to 0.8–1.6 MWe for vertical and deviated systems.
- Formation temperature analyses indicate that lateral systems distribute thermal drawdown over a larger rock volume, delaying localised thermal exhaustion at the expense of a broader thermal footprint. Across all configurations, injection flow rates above approximately 9 L s^{-1} accelerate near-well cooling and reduce long-term outlet temperature, highlighting the importance of balanced flow-rate selection.
- Insulation effects are time-dependent and most effective during early operation. For coaxial systems, inner-pipe insulation is the primary mechanism for mitigating internal thermal short-circuiting, while outer-pipe insulation provides secondary benefits, particularly for long or horizontal geometries.

Overall, the findings underscore trajectory optimisation and lateral exposure to high-temperature formations as the most effective design strategies for closed-loop geothermal deployment in shallow volcanic environments. Future research should focus on advanced carrier fluids (e.g., nanofluids, CO_2), intermittent operation for a sustainable geothermal heat recovery considering thermal interference in multi-well systems. Furthermore, future work should incorporate fracture-controlled heat transfer, thermo-hydraulic coupling at the reservoir scale, and economic assessments to further refine system design and feasibility.

Ethics approval and consent to participate

Not applicable

Consent for publication

Not applicable

Availability of data and materials

The datasets used and/or analysed during the current study are available from the corresponding author on reasonable request.

Competing interests

The authors declare that they have no competing interests

Funding

This study was carried out within the framework of the PhD fellowship of the 38th cycle, funded by the Istituto Nazionale di Geo- fisica e Vulcanologia (INGV).

Acknowledgements

Not applicable

CRediT authorship contribution statement

Dan Azimi Mohaman: Conceptualization, Methodology, Visualization, Validation, Formal analysis, writing – original draft, Writing – review & editing. **Monia Procesi:** review & editing, Supervision. **Eloisa Di Sipio:** Methodology, review & editing. **Giorgia Dalla Santa:** Methodology, review & editing. **Paolo Scotton:** review & editing. **Antonio Galgaro:** Conceptualization, Methodology, Formal analysis, review & editing, Visualization, Validation, Supervision.

References

[1] Durga S, Beckers KF, Taam M, Horowitz F, Cathles LM, Tester JW. Techno-economic analysis of decarbonizing building heating in upstate New York using seasonal borehole thermal energy storage. Energy Build. 2021;241: 110890.

[2] Gluyas J, Adams C, Busby J, Craig J, Hirst C, Manning D, McCay A, Narayan N, Robinson H, Watson S, et al. Keeping warm: a review of deep geothermal potential of the UK. Proc Inst Mech Eng A J Power Energy. 2018;232(1):115–26.

[3] GENI. (2008). Renewable energy potential of small island states. Global Energy Network Institute. Retrieved from https://www.geni.org/globalenergy/library/articles-renewable-energy-transmission/small-island-nations.shtml.

[4] Kuang, Y., Zhang, Y., Zhou, B., Li, C., Cao, Y., Li, L., & Zeng, L. (2016). A review of renewable energy utilization in islands. Renewable and Sustainable Energy Reviews, 59, 504–513. https://doi.org/10.1016/j.rser.2016.01.014.

[5] Nakomcic-Smaragdakis, B., Dvornic, T., Cepic, Z., & Dragutinovic, N. (2016). Analysis and possible geothermal energy utilization in a municipality of Panonian Basin of Serbia. Renewable and Sustainable Energy Reviews, 59, 940–951. https://doi.org/10.1016/j.rser.2015.12.337.

[6] Soltani, M., Kashkooli, F. M., Dehghani-Sanij, A. R., Kazemi, A. R., Bordbar, N., Farshchi, M. J., Elmi, M., Gharali, K., & Dusseault, M. B. (2019). A comprehensive study of geothermal heating and cooling systems. Sustainable Cities and Society, 44, 793–818. https://doi.org/10.1016/j.scs.2018.09.036.

720 [7] Wang, G., Song, X., Shi, Y., Fei, Y., Yang, R., & Li, J. (2020). Comparison of production
721 characteristics of various coaxial closed-loop geothermal systems. Energy Conversion and
722 Management, 225, 113437. https://doi.org/10.1016/j.enconman.2020.113437.

723 [8] Glassley, W. E. (2014). Geothermal energy: Renewable energy and the environment (2nd
724 ed.). CRC Press. Retrieved from https://books.google.it/books?id=hPCsBAAAQBAJ.

725 [9] Shi, Y., Song, X., Wang, G., Li, J., Geng, L., & Li, X. (2019). Numerical study on heat
726 extraction performance of a multilateral-well enhanced geothermal system considering
727 complex hydraulic and natural fractures. Renewable Energy, 141, 950–963.
728 https://doi.org/10.1016/j.renene.2019.03.142.

729 [10] Pruess, K. (2006). Enhanced geothermal systems (EGS) using CO2 as working fluid-A
730 novel approach for generating renewable energy with simultaneous sequestration of carbon.
731 Geothermics, 35(4), 351–367. https://doi.org/10.1016/j.geothermics.2006.08.002.

732 [11] Chen, Y., Ma, G., Wang, H., Li, T., & Wang, Y. (2019). Application of carbon dioxide as
733 working fluid in geothermal development considering a complex fractured system. Energy
734 Conversion and Management, 180(September 2018), 1055–1067.
735 https://doi.org/10.1016/j.enconman.2018.11.046.

736 [12] Giardini, D. (2009). Geothermal quake risks must be faced. Nature, 462(7275), 848–849.
737 https://doi.org/10.1038/462848a.

738 [13] Anderson, A., & Rezaie, B. (2019). Geothermal technology: Trends and potential role in
739 a sustainable future. Applied Energy, 248(April), 18–34.
740 https://doi.org/10.1016/j.apenergy.2019.04.102.

741 [14] Wang, G., Song, X., Shi, Y., Yang, R., Yulong, F., Zheng, R., & Li, J. (2021). Heat
742 extraction analysis of a novel multilateral-well coaxial closed-loop geothermal system.
743 Renewable Energy, 163, 974–986. https://doi.org/10.1016/j.renene.2020.08.121.

744 [15] Holmberg, H., Acuña, J., Næss, E., Sønju, O.K. (2016). Thermal evaluation of coaxial
745 deep borehole heat exchangers Acu n. 97, 65–76. https://doi.org/10.1016/j.renene.2016.05.048.

746 [16] Dai, C., Li, J., Shi, Y., Zeng, L., & Lei, H. (2019). An experiment on heat extraction from
747 a deep geothermal well using a downhole coaxial open-loop design. Applied Energy, 252,
748 113447. https://doi.org/10.1016/j.apenergy.2019.113447.

749 [17] Wang, G., Song, X., Shi, Y., Sun, B., Zheng, R., Li, J., Pei, Z., & Song, H. (2019).
750 Numerical investigation on heat extraction performance of an open-loop geothermal system in
751 a single well. Geothermics, 80, 170–184. https://doi.org/10.1016/j.geothermics.2019.03.005.

752 [18] Wang, G., Song, X., Shi, Y., Zheng, R., Li, J., & Li, Z. (2020). Production performance
753 of a novel open-loop geothermal system in a horizontal well. Energy Conversion and
754 Management, 206, 112478. https://doi.org/10.1016/j.enconman.2020.112478.

755 [19] Wang, G., Song, X., Yu, C., Shi, Y., Song, G., Xu, F., Ji, J., & Song, Z. (2022). Heat
756 extraction study of a novel hydrothermal open-loop geothermal system in a multi-lateral
757 horizontal well. Energy, 242, 122527. https://doi.org/10.1016/j.energy.2021.122527.

758 [20] Yu, P., Dempsey, D., & Archer, R. (2021). A three-dimensional coupled thermo-hydro-
759 mechanical numerical model with partially bridging multi-stage contact fractures in horizontal-
760 well enhanced geothermal system. International Journal of Rock Mechanics and Mining
761 Sciences, 143, 104787. https://doi.org/10.1016/j.ijrmms.2021.104787.

762 [21] Xie, J., Wang, J., & Liu, X. (2022). Performance analysis of pinnate horizontal well in
763 enhanced geothermal system. Applied Thermal Engineering, 201, 117799.
764 https://doi.org/10.1016/j.applthermaleng.2021.117799.

765 [22] Pasqualetti M. Geothermal energy and the environment: the global experience. Energy.
766 1980;5(2):111–65.

767 [23] Bayer P, Rybach L, Blum P, Brauchler R. Review on life cycle environmental effects of
768 geothermal power generation. Renew Sustain Energy Rev. 2013; 26:446–63.
769 https://doi.org/10.1016/j.rser.2013.05.039.

770 [24] Soltani M, Kashkooli FM, Souri M, Rafiei B, Jabarifar M, Gharali K, Nathwani JS.
771 Environmental, economic, and social impacts of geothermal energy systems. Renew Sustain
772 Energy Rev. 2021;140: 110750. https://doi.org/10.1016/j.rser.2021.110750.

773 [25] Wang, Z., Wang, F., Liu, J., Ma, Z., Han, E., & Song, M. (2017). Field test and numerical
774 investigation on the heat transfer characteristics and optimal design of the heat exchangers of
775 a deep borehole ground source heat pump system. Energy Conversion and Management, 153,
776 603–615. https://doi.org/10.1016/j.enconman.2017.10.038.

777 [26] Renaud, T., Verdin, P., & Falcone, G. (2019). Numerical simulation of a deep borehole
778 heat exchanger in the Krafla geothermal system. International Journal of Heat and Mass
779 Transfer, 143, 118496. https://doi.org/10.1016/j.ijheatmasstransfer.2019.118496.

780 [27] Zhang, Y., Yu, C., Li, G., Guo, X., Wang, G., Shi, Y., Peng, C., & Tan, Y. (2019).
781 Performance analysis of a downhole coaxial heat exchanger geothermal system with various
782 working fluids. Applied Thermal Engineering, 163, 114317.
783 https://doi.org/10.1016/j.applthermaleng.2019.114317.

784 [28] Luo, Y., Shen, J., Song, Y., Liu, Q., Huo, F., Chu, Z., & Liu, A. (2024). Multi-segmented
785 tube design and multi-objective optimization of deep coaxial borehole heat exchanger.
786 Renewable Energy, 237, 121494. https://doi.org/10.1016/j.renene.2024.121494.

787 [29] Guo, Z., Dai, Y., Zhang, J., Gui, X., & He, Y. (2024). Improved modeling analysis on heat
788 transfer performance of deep coaxial borehole heat exchanger with different operation modes.
789 Energy Reports, 11, 355–368. https://doi.org/10.1016/j.egyr.2023.11.066.

790 [30] Bai, M., Wang, F., Liu, J., Cai, W., & Wang, Z. (2022). Discrepancies in using CO_2 or
791 water as heat-carrier fluid on the output temperature of deep coaxial borehole heat exchanger.
792 Energy and Buildings, 270, 112279. https://doi.org/10.1016/j.enbuild.2022.112279.

793 [31] Deng, J., Peng, C., Su, Y., Qiang, W., Cai, W., & Wei, Q. (2023). Research on the heat
794 storage characteristic of deep borehole heat exchangers under intermittent operation mode:
795 Simulation analysis and comparative study. Energy, 282, 128938.
796 https://doi.org/10.1016/j.energy.2023.128938.

797 [32] Song, X., Wang, G., Shi, Y., Li, R., Xu, Z., Zheng, R., Wang, Y., & Li, J. (2018).
798 Numerical analysis of heat extraction performance of a deep coaxial borehole heat exchanger
799 geothermal system. Energy, 164, 1298–1310. https://doi.org/10.1016/j.energy.2018.08.056.

800 [33] Beckers, K. F., Rangel-Jurado, N., Chandrasekar, H., Hawkins, A. J., Fulton, P. M., &
801 Tester, J. W. (2022). Techno-economic performance of closed-loop geothermal systems for
802 heat production and electricity generation. Geothermics, 100, 102318.
803 https://doi.org/10.1016/j.geothermics.2021.102318.

804 [34] Liu, Q., Zhang, Y., Luo, J., Zheng, J., & Cheng, Y. (2023). Numerical study on heat
805 transfer and flow characteristics of coaxial geothermal heat exchangers with helical finned

inner tubes. Journal of Building Engineering, 65, 105752. https://doi.org/10.1016/j.jobe.2022.105752.

[35] Liu, Q., Zhang, Y., Zhang, X., Luo, J., Zheng, J., Liu, Y., & Lou, J. (2024). Numerical study on the heat transfer performance evaluation, flow characteristics, exergy efficiency, and entropy generation analysis of a novel coaxial geothermal heat exchanger. Journal of Building Engineering, 84, 108555. https://doi.org/10.1016/j.jobe.2024.108555.

[36] Liu, Q., Zhang, Y., Zhang, X., Cheng, Y., Luo, J., Zheng, J., & Lou, J. (2023). Numerical study on a coaxial geothermal exchanger equipped with a new inner tube: Entropy generation, thermodynamic irreversibility analysis and exergy efficiency performance evaluation. Journal of Cleaner Production, 424, 138803. https://doi.org/10.1016/j.jclepro.2023.138803.

[37] Rajeh, T., Al-Kbodi, B. H., Yang, L., Zhao, J., & Zayed, M. E. (2023). A novel oval-shaped coaxial ground heat exchanger for augmenting the performance of ground-coupled heat pumps: Transient heat transfer performance and multi-parameter optimization. Journal of Building Engineering, 79, 107781. https://doi.org/10.1016/j.jobe.2023.107781.

[38] Rajeh, T., Al-Kbodi, B. H., Zayed, M. E., Li, Y., Zhao, J., & Rehman, S. (2024). Local entropy generation optimization and thermodynamic irreversibility analysis of oval-shaped coaxial ground heat exchangers: A detailed numerical investigation. International Journal of Heat and Mass Transfer, 228, 125650. https://doi.org/10.1016/j.ijheatmasstransfer.2024.125650.

[39] Mao, L., & Zhang, Z. (2018). Transient temperature prediction model of horizontal wells during drilling shale gas and geothermal energy. Journal of Petroleum Science and Engineering, 169, 610–622. https://doi.org/10.1016/j.petrol.2018.05.069.

828 [40] Akram, W., Chen, Q., Nortz, G., & Nortz, P. (2024). Experimental investigation and
829 numerical modeling of an innovative horizontal coaxial ground heat exchanger (HCGHE) for
830 geothermal heat pump applications. Applied Thermal Engineering, 257, 124492.
831 https://doi.org/10.1016/j.applthermaleng.2024.124492.

832 [41] Wang, G., Song, X., Song, G., Shi, Y., Yu, C., Xu, F., Ji, J., & Song, Z. (2021). Analysis
833 of thermal characteristics of a hydrothermal coaxial closed-loop geothermal system in a
834 horizontal well. International Journal of Heat and Mass Transfer, 180, 121755.
835 https://doi.org/10.1016/j.ijheatmasstransfer.2021.121755.

836 [42] Liu, Y., Li, K., Guan, Z., Lin, G., & Xu, Y. (2023). Research on circulating heat recovery
837 law of single horizontal well for hot dry rock geothermal resources. Renewable Energy, 217,
838 119108. https://doi.org/10.1016/j.renene.2023.119108.

839 [43] Liu, S., Taleghani, A. D., & Ji, K. (2024). An advanced closed-loop geothermal system to
840 substantially enhance heat production. Energy Conversion and Management, 322, 119168.
841 https://doi.org/10.1016/j.enconman.2024.119168.

842 [44] Esmaeilpour, M., Korzani, M. G., & Kohl, T. (2023). Stochastic performance assessment
843 on long-term behavior of multilateral closed deep geothermal systems. Renewable Energy,
844 208, 26–35. https://doi.org/10.1016/j.renene.2023.03.074.

845 [45] Kelly, J. J., & Mcdermott, C. I. (2022). Numerical modelling of a deep closed-loop
846 geothermal system : evaluating the Eavor-Loop. 8(February), 175–212.
847 https://doi.org/10.3934/geosci.2022011.

848 [46] Sommaruga, C., 1984. Le ricerche geotermiche svolte a Vulcano negli anni ‘50. In:
849 Rendiconti della Società Italiana di Mineralogia e Petrologia. 39. pp. 355–366.

[47] Todesco, M. (1995). Modeling of the geothermal activity at Vulcano (Aeolian islands, Italy). Proceedings of the World Geothermal Congress, 2(January 1995), 1309–1314.

[48] Mohaman D.A., Procesi M., Di Sipio E., Dalla Santa G., Scotton P., Galgaro A, Evaluation of a Closed-Loop coaxial borehole heat exchanger in High-Temperature volcanic environment, Energy Conversion and Management: X (2025), doi: https://doi.org/10.1016/j.ecmx.2025.101388.

[49] Teodoriu, C., & Bello, O. (2021). An outlook of drilling technologies and innovations: Present status and future trends. In Energies (Vol. 14, Issue 15). MDPI AG. https://doi.org/10.3390/en14154499.

[50] Eren, T., & Suicmez, V. S. (2020). Directional drilling positioning calculations. Journal of Natural Gas Science and Engineering, 73. https://doi.org/10.1016/j.jngse.2019.103081.

[51] Wísniowski, R., Łopata, P., & Orłowicz, G. (2020). Numerical methods for optimization of the horizontal directional drilling (HDD)well path trajectory. Energies, 13(15). https://doi.org/10.3390/en13153806.

[52] COMSOL Multiphysics Reference Manual. https://doc.comsol.com/6.1/doc/com.comsol.help.comsol/COMSOL_ReferenceManual.pdf.

[53] Pryor, R. W. (2011). Multiphysics modeling using COMSOL : a first principles approach. Jones and Bartlett Publishers.

[54] Haaland, S. E. (March 1, 1983). "Simple and Explicit Formulas for the Friction Factor in Turbulent Pipe Flow." ASME. J. Fluids Eng. March 1983; 105(1): 89–90.https://doi.org/10.1115/1.3240948.

[55] Gnielinski, V. (1976). New equations for heat and mass transfer in turbulent pipe and channel flow. International Chemical Engineering, 16, 359–368.

[56] Gola, G., Di Sipio, E., Facci, M., Galgaro, A., & Manzella, A. (2022). Geothermal deep closed-loop heat exchangers: A novel technical potential evaluation to answer the power and heat demands. Renewable Energy, 198, 1193–1209. https://doi.org/10.1016/j.renene.2022.08.071.

[57] Huajun, W., Yishuo, X., Yukun, S., & Sumin, Z. (2022). Heat extraction by deep coaxial borehole heat exchanger for clean space heating near Beijing, China: Field test, model comparison and operation pattern evaluation. Renewable Energy, 199(August), 803–815. https://doi.org/10.1016/j.renene.2022.09.017.

[58] Armstrong, J. Scott, and Fred Collopy. "Error Measures for Generalizing about Forecasting Methods: Empirical Comparisons." International Journal of Forecasting., vol. 8, no. 1, 1992, pp. 69–80, https://doi.org/10.1016/0169-2070(92)90008-W.

[59] Kim, S., & Kim, H. (2016). A new metric of absolute percentage error for intermittent demand forecasts. International Journal of Forecasting, 32(3), 669–679. https://doi.org/10.1016/j.ijforecast.2015.12.003.

[60] Caulk, R. A., & Tomac, I. (2017). Reuse of abandoned oil and gas wells for geothermal energy production. Renewable Energy, 112, 388–397. https://doi.org/10.1016/j.renene.2017.05.042.